MASTER'S THESIS

Course code: BIO5010 Name: Marit By

Reindeer cadavers alter vegetation composition in the Arctic tundra of Svalbard

Date: 16.05.22 Total number of pages: 55

NORD University

www.nord.no

Reindeer cadavers alter vegetation composition in the Arctic tundra of Svalbard

Reinsdyrkadaver endrer vegetasjonssammensetningen i den Arktiske tundraen på Svalbard

Photos: Marit By

Marit By
marit-by@outlook.com

Supervisors:

Sam Steyaert
sam.steyaert@nord.no
Nord University

Rakel Blaalid
rakel.blaalid@uib.no
University of Bergen

Jan Eivind Østnes
jan.e.ostnes@nord.no
Nord University

Master in Biosciences: Terrestrial Ecology and Nature Management
Faculty of Biosciences and Aquaculture, Nord University

Steinkjer, 16.05.2021

Abstract

Nutrient cycling of organic matter is a crucial process in ecosystems. Cadavers provide a nutrient flow into the ecosystem and form “cadaver decomposition islands” (CDI). These CDI`s can be considered as nutrient hotspots as the cadaver provide important nutrients like nitrogen and phosphorus. In nutritionally marginal areas far north, such as the Arctic tundra, nutrient turnover is slow. The supply of nutrients therefore has a great impact on vegetation growth. Due to poor snow conditions many Svalbard reindeer die from starvation and avalanches. Decomposition of these cadavers provides a major impact on the vegetation.

Drone has made their entrance into ecological research in recent times. In vegetation studies, they can be equipped with traditional RGB cameras, multispectral cameras, or other types of sensors. The images collected from the drones makes is possible to calculate different vegetation indices (e.g. Green Leaf Index) to map the condition of the vegetation.

The overall aim of this study is to assess how reindeer cadavers affect vegetation cover and composition in the Arctic tundra in space and time. There were carried out a ground survey and drone survey of the vegetation late summer 2021, at 33 cadaver sites (from 2017 to 2021) with 33 paired control sites. The ground survey was done within a grid of 5 x 5 m, with sub-squares of 1 m. For all the sub-squares I registered percentage cover of woody plants, graminoids, herbs, bryophytes, lichen, bare soil, cadaver material and rocks. In the drone survey I collected RGB images at 30 m, 50 m, and 100 m altitude. The ground survey data were analyzed using both Wilcoxon Signed Rank Test and Generalized Linear Mixed Models. From the drone images I calculated various RGB based vegetation indices and analyzed whether or not these indices differed between cadaver and control sites using Wilcoxon Signed Rank tests.

The first year of the study the woody plants showed higher cover at cadaver sites, while the herbs showed lower cover at cadaver sites. Graminoids showed higher cover at cadaver sites during the entire study. Bryophytes and lichen showed lower cover at cadaver sites during the entire study. The response was generally stronger at the core of the cadaver sites and deceased towards the outer part of the grid.

The Modified Green Red Vegetation Index showed high index values in cadaver sites indicated increased chlorophyll production for all years and altitudes. The Green Leaf Index showed low index values at cadaver sites the first year, and high index values from the second year. This was shown from all altitudes.

Sammendrag

Sirkulering av organisk materiale er en avgjørende prosess i økosystemer. Kadaver gir en næringsstrøm inn i økosystemet og danner kadavernedbrytningsøyer (CDI). Disse CDI-ene kan betraktes som nærings-hotspots ved at de tilfører viktige næringsstoffer til omgivelsene, spesielt nitrogen og fosfor. I marginale områder langt nord, som den arktiske tundraen, går næringsomsetningen sakte. Tilførselen av næringsstoffer har derfor stor innvirkning på vegetasjon. Under dårlige snøforhold dør mange Svalbardrein på grunn av sult og snøskred. Nedbryting av disse kadavrene kan dermed ha påvirkning på vegetasjonen.

Droner er et verktøy som har gjort sitt inntog i forskningen i nyere tid. I vegetasjonsstudier kan droner brukes både med RGB-kameraer, multispektrale kameraer eller andre typer sensorer. Bildene samlet inn fra dronene gjør det mulig å beregne ulike vegetasjonsindekser (f.eks. Green Leaf Index) for å kartlegge tilstanden til vegetasjonen.

Det overordnede målet med denne studien er å vurdere hvordan reinsdyrkadaver påvirker vegetasjonsdekket og sammensetningen i den arktiske tundraen i rom og tid. Det ble gjennomført en bakkeundersøkelse og droneundersøkelse av vegetasjonen sensommeren 2021, på 33 kadaverlokaliteter (fra 2017 til 2021) med 33 parede kontroll-lokaliteter. Bakkeundersøkelsen ble gjort innenfor et rutenett på 5 x 5 m, med delruter på 1 m. For alle delrutene registrerte jeg prosentvis dekning av forvedete planter, graminoider, urter, moser, lav, bar jord, kadavermateriale og stein. I droneundersøkelsen samlet jeg RGB-bilder i 30 m, 50 m og 100 m høyde. Bakkeundersøkelsesdataene ble analysert ved bruk av både Wilcoxon Signed Rank Test og Generalized Linear Mixed Models. Fra dronebildene beregnet jeg forskjellige RGB-baserte vegetasjonsindekser og analyserte hvorvidt disse indeksene var forskjellig mellom kadaver og kontroll-lokaliteter ved å bruke Wilcoxon Signed Rank tester.

Det første året av studien viste de forvedete plantene et høyere dekke på kadaverlokaliteter, mens urtene viste et lavere dekke. Graminoider viste høyere dekning på kadaverlokaliteter under hele studien. Moser og lav viste lavere dekke ved kadaverlokaliteter under hele studien. Responsen var generelt sterkere i sentrum av kadaverlokalitetene og avtok mot kanten av rutenettet.

Modified Green Red Vegetation Index viste høye indeksverdier på kadaverlokaliteter, og indikerte økt klorofyllproduksjon for alle år og flyhøyder. Green Leaf Index viste lave indeksverdier på kadaverlokaliteter det første året, og høye indeksverdier på det andre året. Dette var gjeldende for alle flyhøyder.

Acknowledgements

Denne masteroppgaven markerer slutten på studiet *Biovitenskap med spesialisering innen terrestrisk økologi og naturforvaltning* ved Nord universitet i Steinkjer. Gjennom arbeidet med oppgaven har jeg fått muligheten til å lære mye om kadaverøkologi, Arktisk tundra og droner. Jeg fikk også gleden av å besøke og utforske Svalbard i forbindelse med feltarbeid. Det har vært et lærerikt år med opp- og nedturer, og det er med stor glede jeg nå har lyktes med å fullføre utdanningen min.

En takk rettes til min hovedveileder Sam Steyaert, førsteamanuensis ved Nord Universitet, for muligheten til deltakelse i kadaver-prosjektet, for hjelp med planlegging av feltarbeid og veiledning i skriveprosessen. Videre vil jeg takke min veileder Rakel Blaalid, forsker ved Universitetsmuseet i Bergen ved avdeling for naturhistorie, for hjelp med feltarbeid, motivasjons-booster og veiledning i skriveprosessen. Jeg vil også takke min veileder Jan Eivind Østnes, førsteamanuensis ved Nord Universitet, for «good mood» i felt, og for veiledning i skriveprosessen. En takk rettes også til Oddbjørn Larsen, overingeniør ved Nord Universitet, for uvurderlig bærehjelp i felt og droneteknisk kompetanse.

I tillegg vil jeg takke mine klassekamerater for mye sprell og moro i løpet av disse to årene både i felt, klasserom og på master-rommet. Jeg vil takke familien min for tålmodighet, økonomisk støtte og godhjertet pushing gjennom seks års utdanning. En stor takk rettes til Inga Frøseth Rossing for korrekturlesing, støtte og mange humørfylte kvelder. Sist, men ikke minst vil jeg takke «gutta boys», Baro Moslet og Jørgen Elstad, for uvurderlig støtte, faglige diskusjoner, latter, trøst, uglelytting, elgsafari og hytteturer i en lang prosess.

Nå går veien videre inn i arbeidslivet.

Marit By
Steinkjer
Mai 2022

Index

1 Introduction

Nutrient cycling of organic matter is a crucial process in ecosystems (Barton et al., 2012; Newsome et al., 2021; Parmenter & MacMahon, 2009). Cadavers can play a disproportionately large role in the nutrient cycling by the nutrient flow they provide into the environment as a result of decomposition (Barton et al., 2012; Barton et al., 2019; Barton et al., 2016; Carter et al., 2006; Newsome et al., 2021; Parmenter & MacMahon, 2009). Decomposition of cadavers was in the early 2000s stated as a neglected microsere (Carter et al., 2006). Since then, however, the impact of cadaver decomposition on ecosystems has been given more attention, but knowledge about how the environment is affected by carrion is still relatively scarce (Barton et al., 2019). In the northernmost latitudes, and especially on the Arctic tundra, the nutrient input in the landscape is often small, and the turnover is low (Danell et al., 2002; Jonasson & Shaver, 1999). The addition of nutrients to the Arctic tundra through cadaver decomposition can therefore have a strong impact on the ecosystem (Danell et al., 2002; Street et al., 2015).

The Arctic tundra of Svalbard hosts only three native species of mammals, namely polar bears (*Ursus maritimus*), Svalbard reindeer (*Rangifer tarandus platyrhynchus*), arctic foxes (*Vulpes lagopus*), and one alien species, the sibling vole (*Microtus levis*) (Hansen et al., 2019; Reimers, 2012). The Svalbard reindeer is the only large mammalian herbivore and experiences little predation from the polar bears (Hansen et al., 2019; Reimers, 2012). Mortality predominantly occurs because of starvation during winters, especially winters with rain on snow events (Hansen et al., 2019; Le Moullec et al., 2019; Reimers, 2012). Mortality can also be caused by avalanches (Nybakk et al., 2002). Cadaver material that is not consumed by scavengers will be left in the landscape to decompose and adds nutrients to the environment (Carter et al., 2006; Reed, 1958). Cadaver often form “cadaver decomposition islands” (CDI) i.e. locations at which high concentrations of nutrients and disturbance by insects and scavengers can remove the vegetation and change the biotic and abiotic conditions (Carter et al., 2006). As a result of this decomposition process, high concentrations of nitrogen and phosphorus will be added to the substrate, which in turn can affect various ecological communities and induce secondary succession (Prach et al., 2019) and can lead to a landscape with increased heterogeneity and complexity (Barton et al., 2019; Bump et al., 2009; Carter et al., 2006; Towne, 2000). Van Klink et al. (2020) found a strong connection between cadaver decomposition and increasing plant biomass around red deer (*Cervus elaphus*) cadavers in the Netherlands, underpinning the cadaver ecosystem effects. From

earlier studies in prairie, Arctic tundra, and forests ecosystems it is known that disturbance like nutritious hotspots induced by cadaver decomposition increase both the diversity and heterogeneity in the ecosystem (Barton et al., 2012; Barton et al., 2019; Bump et al., 2009; Carter et al., 2006; Danell et al., 2002; Melis et al., 2007). However, this response have been reported to occur only a few meters from the center of the cadaver (Danell et al., 2002).

The Arctic tundra is characterized by a low average temperature in the warmest months (< 10°C), and a growing season that is too short for trees to establish (Lee, 2020). Another important characteristic of the Arctic tundra is permafrost (Lee, 2020; Rouyet et al., 2019). Permafrost is defined by frozen soil during the entire year and consists of a vegetated layer (active layer) (Lee, 2020; Rouyet et al., 2019). The thickness of the active layer limits the root systems, modulates the height of the vegetation, and determines access to nutrients (Lee, 2020). Due to various reasons, such as climate and warm and cold sea streams, the Arctic tundra can be at different latitudes around the world (Lee, 2020). The Arctic tundra on Svalbard is relatively mild for its latitude because of the influence of the Gulf Stream, especially in the western parts (Hansen et al., 2019). On the eastern side the archipelago is more influenced by the sea-ice cover (Hansen et al., 2019).

Due to the low temperatures and limited depth of the active layer, the Arctic tundra is a demanding habitat for vegetation (Lee, 2020; Wang et al., 2018). Changes in the supply of nutrients have therefore been shown to result in significant changes in the plant growth (Wang et al., 2018). Cadaver decomposition may thus have a pronounced impact on the ecology of the Arctic tundra, for example by improving growth conditions for plants by adding nutrients (Danell et al., 2002). Both nitrogen and phosphorus regulate many processes on the Arctic tundra, including the species composition, and therefore have a key role in such ecosystems (Barton et al., 2019; Fremstad, 1992). Increased supply of the nutrients generally leads to increased plant production, but with a transient surplus; i. e. the increased growth and production will cease at some point, and in some cases the concentration of nutrients may become lethal (Carter et al., 2006; Fremstad, 1992). Previous studies of vegetation responses due to nitrogen supply have shown large variations across different plant groups (Fremstad, 1992; Soudzilovskaia et al., 2005; van Klink et al., 2020). Woody plants have proven to benefit from initial nitrogen supply (Martin et al., 2022), but if the supply occurs repeatedly a reduction in cover can occur (Fremstad, 1992). Herbs and graminoids are able to take advantage of an increased supply of nitrogen (Bump et al., 2009; Towne, 2000), and can thereby outcompete other species (Fremstad, 1992). Notably, graminoids have also been

demonstrated to increase in biomass at cadaver sites (van Klink et al., 2020). For lichen and bryophytes, previous studies show opposite trends. Soudzilovskaia et al. (2005) showed that nitrogen supply leads to a large decrease in the biomass of lichen. Bryophyte responses to nutrient supplies may vary. Fremstad (1992), for example, reported a trend of decrease in bryophyte cover due to nitrogen supply , whereas Sun et al. (2017) reported the opposite.

Vegetation studies typically rely on field surveys to register species composition, biomass, or the condition of the vegetation (Guan et al., 2019; Li et al., 2018; Olson et al., 2019). Unmanned aerial vehicles or drones have recently become an important tool for studies related to vegetation ecology and ecology in general (Guan et al., 2019; Li et al., 2018; Olson et al., 2019). Drones are tools that can be used to obtain fast and affordable imagery with high spatial resolution (Guan et al., 2019; Li et al., 2018; Olson et al., 2019). They can be equipped with a variety of different sensors and are flexible in timing for detecting different stages in vegetation without disturbance of clouds or atmospheric particles, which typically hamper satellite imaging (Torresan et al., 2017). Nevertheless, drones have a relatively short flight time, and they are often sensitive to too high and too low temperatures, wind and rain (Wich & Koh, 2018). The European Union has also drawn up a set of rules that regulate drone operations and requires pilot certification (European Union Aviation Safety Agency, 2021). The use of drones as a platform for both traditional Red, Green, and Blue (RGB) and multispectral vegetation mapping has gained substantial importance in recent years (Astor et al., 2020). Using drones to collect imagery in different wavelengths gives an opportunity to calculate spectral indices that can be used to investigate vegetation characteristics (De Swaef et al., 2021; Guan et al., 2019; Olson et al., 2019; Yao et al., 2017). Some vegetation index studies used RGB cameras attached to the drone (De Swaef et al., 2021; Yao et al., 2017), which capture images in the visible part (i.e. red, 650nm; green, 550nm; blue 450nm) of the electromagnetic spectrum (Neumann et al., 2021; Yao et al., 2017). The Modified Green Red Vegetation Index (MGRVI), Red Green Blue Vegetation Index (RGBVI), and Green Leaf Index (GLI) are examples of indices that can easily be calculated from the standard RGB cameras (Louhaichi et al., 2001; Neumann et al., 2021; Pettorelli et al., 2005). The GLI is a vegetation index based on the green, red, and blue bands, and emphasizes different reflectance for vegetation and non-vegetated surfaces, and are previously used to detect areas exposed to grazing (Louhaichi et al., 2001) and changes in habitat and vegetation stress estimation (Curran & Williamson, 1987). The MGRVI and RGBVI are indices based at the red and green, and the red, green and blue bands, respectively (Neumann et al., 2021). The MGRVI

has been used to estimate vegetation biomass (Wan et al., 2018), and the RGBVI for monitoring vegetation growth (Bareth et al., 2016). Traditional field surveys on the ground can provide a lot of information about the structure and cover of vegetation in an area. Drone imagery can complement such information with knowledge about the lushness of the vegetation.

The overall aim of this study is to assess how reindeer cadavers affect vegetation cover and composition in the Arctic tundra in space and time. More specifically I aim to evaluate the following:

Hypothesis 1 - Cadaver has differential impacts on vegetation functional groups (H1). I expect that the cover of woody plants, graminoids, and herbaceous species will increase as a response to cadaver decomposition, whereas lichens and bryophytes will decrease (H1a). I expect that this response will be very local and not extend more than a few meters from the cadaver center (H1b). I expect that lichens and bryophytes will be less abundant at the cadaver center compared to the surroundings (H1c). Furthermore, I expect that vegetation responses of cadavers will only be apparent after one growing season and fade out over time (H1d).

Hypothesis 2 - Cadavers affect the spectral reflectance of vegetation (H2). I expect that the vegetation will be greener due to the nitrogen and phosphorus that presumably is added to the soil, and thus increase the chlorophyll production in the vegetation (H2a). I expect that the CDI will be denuded from vegetation and dominated by cadaver material and hence have lower spectral reflectance than the surroundings (H2b).

2 Methods

2.1 Study area

This study was performed in Adventdalen including the side valleys Endalen, Todalen, Bolterdalen, and in Bjørndalen and Hjorthamn at Spitsbergen (78°N 18°E), Svalbard archipelago (Figure 1). The landscape is complex and extends from sea level to mountains peaks at more than 1000 meters above sea level (Rouyet et al., 2019). Svalbard airport measures an annual mean temperature of -6.7°C, and a mean summer temperature (July to august) of 5.3°C (Hansen et al., 2019). The annual precipitation is 190 mm and gives a dry yet oceanic climate (Hansen et al., 2019). Only about 15 % of the land area on Svalbard is covered by vegetation (Eischeid et al., 2021; Le Moullec et al., 2019), and consist of the areas in the lowland, the inland valleys, and along the coast (Le Moullec et al., 2019). The remaining 85 % of the area consists of glaciers, bare mountains and bare soil and rock (Johansen et al., 2009). The bioclimatic zones on Svalbard include the Middle Arctic tundra, Northern Arctic tundra, and polar dessert (Blaalid et al., 2014; Johansen et al., 2009; Le Moullec et al., 2019). In Adventdalen, the areas in the valley floors closest to the Advent River are dominated by mires and bryophyte communities, while the vascular plant communities dominates in the more elevated and dry parts of the valley (Tømmervik et al., 2014).

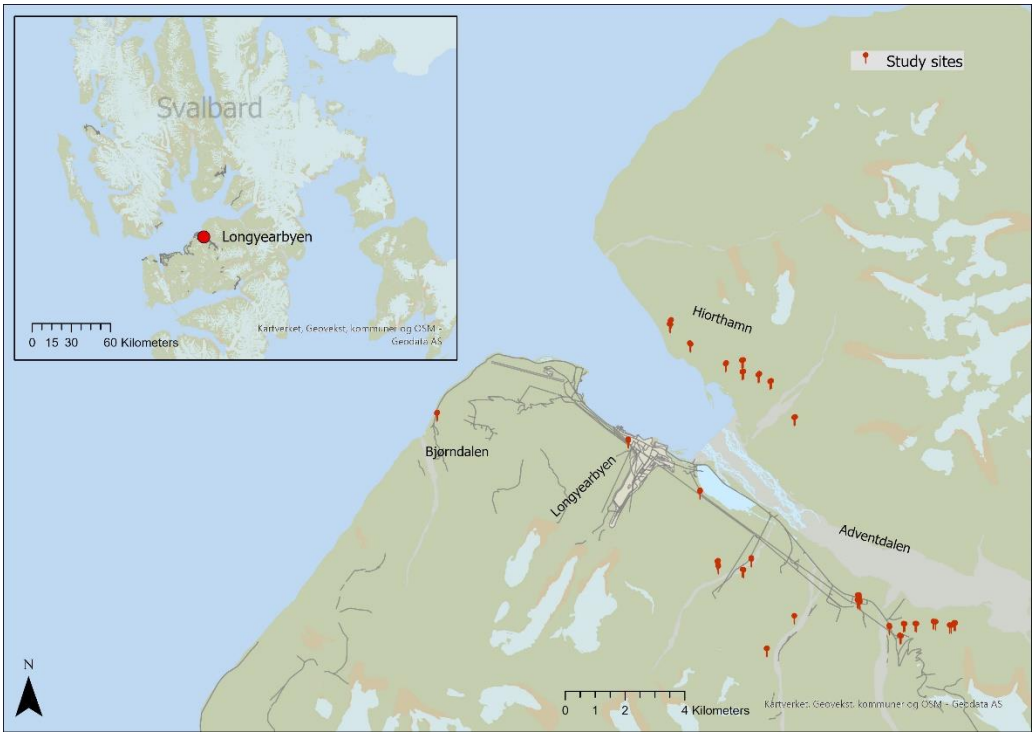

Figure 1: Overview of the study area with each study site indicated with red pins. The inserted map shows the location of the study area on the Svalbard archipelago.

2.2 Data collection

Data were collected in the period from 21 July to 03 August 2021 (Figure 2). A georeferenced dataset of reindeer cadaver from the Norwegian Polar Institute (Hansen et al., 2019; Le Moullec et al., 2019) was used as the base for selecting cadavers included in the study. The criteria for choosing a cadaver were that it should be a maximum of eight km from either a road or a place reachable by boat, and it should also be possible to locate the center of the cadaver (i.e. rumen content, CDI). The age of the cadavers was ranged from 0 to 4 years (i.e., originating between 2017 and 2021).

Figure 2: Fieldwork in Adventdalen consisted of drone flying with DJI matrice 210 (left picture) and conducting vegetation ground surveys (right picture) Photo: Oddbjørn Larsen 25.07.21

At the sites for ground surveys, I made a grid with an area of 5 x 5 m using a mesh made out of rope. The grid was subdivided into 25 1*1 m grid cells and placed with the central cell covering the cadaver center. The control sites were chosen randomly in distance between 30 - 50 m and direction from the cadaver site but had to be in the same vegetation and terrain type as the cadaver. The control sites were surveyed with the same type of grid as the cadaver sites. The total cover (in percent to the nearest 5 %) of cadaver material, bare soil, woody plants, graminoids, herbs, bryophytes, lichen, and rocks were registered for each of the 25 1 x 1 m cell in the grid, as well as for the total square of 5 x 5 m.

The vegetation groups were defined in the following way: 1) woody plants are plants with lignin-containing stems (ericaceous species together with *Betula nana, Salix polaris* and *Dryas octopetala*), 2) graminoids includes member of *Poaceae* and *Cyperaceae,* 3). Herbs are defined as all flowering plants without lignin-containing stems, 4) bryophytes includes all mosses, liverworts, and hornworts, and 5) lichen consists of all lichenized fungal species.

Black and white markers were placed at the grid corners. Two different drones were used to get drone imagery: DJI Mavic Pro 2 with RGB camera and DJI Matrice 210 with both RGB

camera and a multispectral camera (Slant Range) (Table 1). The DJI Matrice 210 was flown over each cadaver and control site at 30 m, 50 m, and 100 m altitude, and collected images with both cameras. The DJI Mavic pro 2 was used together with the app Pix4D (Pix4D AS, 2022) to create a flight route and to collect images for generating orthophotos. The orthophotos were used to georeference the images collected with the DJI Matrice 210.

Table 1: Show the bands of the cameras attached to the drones used in the drone survey.

Camera	DJI Mavic Pro	DJI Matrice 210
RGB	Red – 650 nm	Red – 650 nm
	Green – 550 nm	Green – 550 nm
	Blue – 450 nm	Blue – 450 nm
Multispectral	None	Green – 550 nm
		Red – 650 nm
		Red Edge – 710 nm
		NIR – 850 nm

The images from the multispectral camera on the DJI Matrice 210 were collected with the intention of calculating vegetation indices with the Red Edge and NIR spectral bands. When preprocessing the images, it was discovered that the file format could not be imported and used in R studio without extensive preprocessing. Because of time limitations only the images from the RGB camera on the DJI Matrice 210 were used to calculate vegetation indices.

2.3 Statistical analyzes

The statistical analyzes were carried out in two parts in the software R Studio Version 1.3.1073 (R Core Team, 2022). The threshold for statistical significance was set to $\alpha = 0.05$.

2.3.1 Vegetation data

The first step during the analyzes of the vegetation data was a data exploration to assess underlying assumptions and data structures. There were also some non-recorded values (NA) that had to be considered in the interpretation of the data. I performed a non-parametric test within the analyzes to test hypothesis H1a. The paired Wilcoxon Signed Rank Test was chosen to compare the cover of each vegetation group between cadaver and control sites(Corder & Foreman, 2014), with cover as response variable and type of site (cadaver or control) as explanatory variable. The data used in the test were percent cover of each vegetation group in the 5 x 5 m square (i.e. one observation per square).

Testing H1b, H1c, and H1d needed analyzes at a more detailed level. The data for each 1 x 1 m sub square in the grid was thus included to study how the response variable was distributed within the entire grid (both for cadaver and control). The spatial location of each sub-square in the grids was assigned with “outer”, “inner” or “core” (figure 3), which made it possible to assess the spatial extent of potential cadaver effects on vegetation.

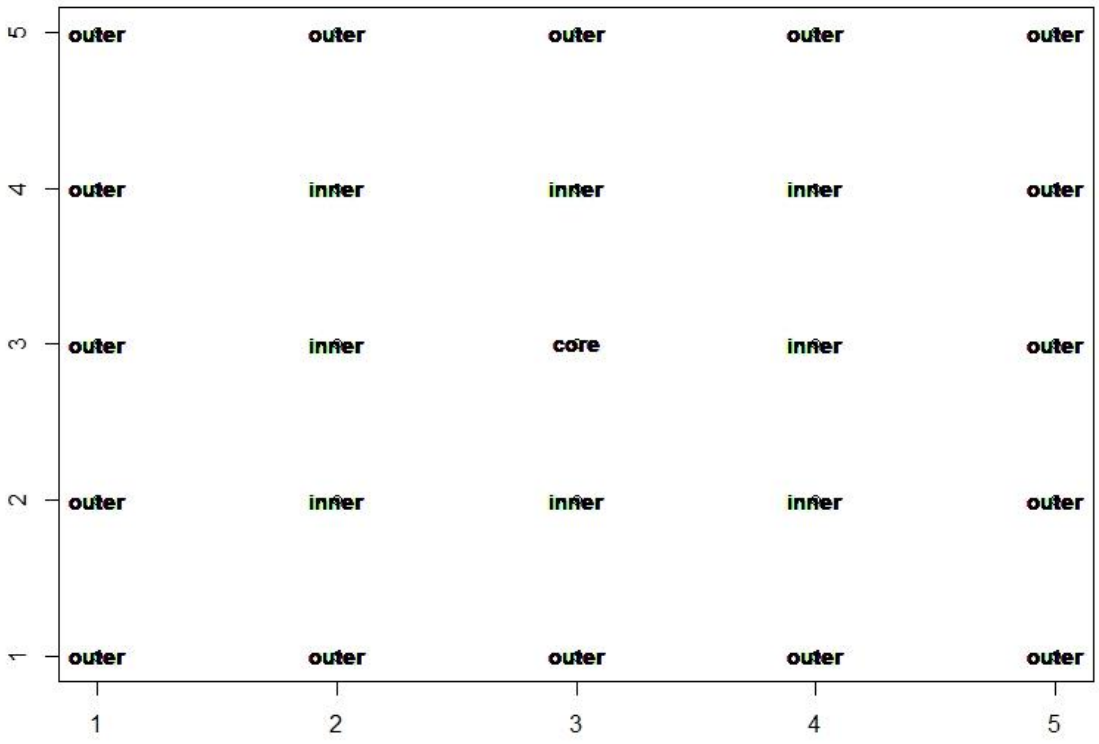

Figure 3: Illustrates the parts of the grid marked with core (1 square), inner (8 square), and outer (16 squares.)

I used generalized linear mixed effect models (glmm) with Template Model Builder (TMB) from the R package glmmTMB (Magnusson et al., 2022). These models include a response variable, explanatory variables and a random variable (Zuur, 2009). The percentage cover of each vegetation group was the response variable. Type (cadaver or control) and band of the grid (core, inner, outer) were the explanatory variables, and the Plot ID were the random variable. The vegetation data was proportion data and was fitted with beta regression using the betareg family with logit link (Magnusson et al., 2022; Zeileis et al., 2021).

To assess changes in the vegetation cover over years at cadaver and control sites I divided the data in ‘new cadavers’ (cadavers from 2021) and ‘old cadavers’ (2017, 2019 and 2020). In this way I was able to assess difference between short time cadaver effects and longer time cadaver effects. There was also a predominance of older cadavers (2019) in the dataset, favoring the divide of the dataset into old and new sites. In total, five model combinations for

each vegetation group for both old and new sites were made; an interaction model (type * band), additive model (type + band), a band only model, a type only model and null model. Site ID was always included as a random factor (Table 2). The best model for each response variable was chosen based on AICc (Akaike Information Criterion corrected for small sample sizes), ΔAICc and the AICcWt. I defined the best model as the one with lowest AICc value, and the highest AICcWt. The ΔAICc show the difference in AICc value between all models and the top ranked model, while the AICcWt assess the level of support the specific model has out of all candidate models.

Table 2: The five glmm models made for each of the vegetation groups and for both new sites and old sites in the statistical analyzes.

Model	Variables
Interaction model	Vegetation cover ~ Type * Band + Site ID
Additive model	Vegetation cover ~ Type + Band + Site ID
Band only model	Vegetation cover ~ Band + Site ID
Type only mode	Vegetation cover ~ Type + Site ID
Null model	Vegetation cover ~ 1 + Site ID

2.3.2 Drone data

To calculate vegetation indices from the drone imagery the raw images needed some preprocessing. First the images collected with the DJI Mavic 2 pro drone and the Pix4D app (Pix4D AS, 2022) were run through the Agifsoft metashape software (Agisoft, 2022), to make one orthophoto for each cadaver and control site pair. The orthophoto for each site was then imported to the software ArcGIS pro (Esri, 2022). In ArcGIS the grids made in field were digitized and converted to shapefiles. The RGB pictures collected with the DJI Matrice 210 were then georeferenced based on the orthophotos and converted to TIFF rasters.

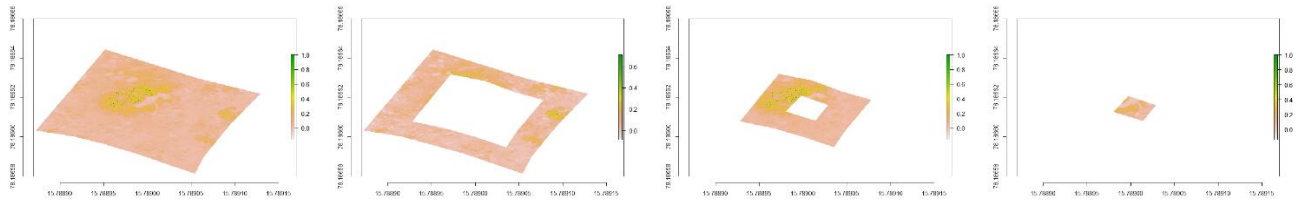

Figure 4: Workflow of the cropping process for total grid, outer, inner and core of the grid. Illustrated with a GLI raster of a cadaver site at 30 m altitude.

The shape file of the grid and the TIFF rasters were loaded into the software R Studio (R Core Team, 2022). In R Studio the rasters were cropped by the outer border of the grid and the three spatial parts of the grid (core, inner and, outer) in the imagery (Figure 4). Three vegetation indices were calculated (Table 3) as mean values for the total grid and for each of the three parts of the grid. The Modified Green Red Vegetation Index (MGRVI) and Red Green Blue Vegetation Index (RGBVI) were calculated to assess differences in chlorophyll absorption between and within cadaver and control sites based on the differences in reflectance in the red, green and blue (Bendig et al., 2015). The plant chlorophyll usually shows high reflectance in the green part of the electromagnetic spectrum, and absorption of red and blue electromagnetic energy (Bendig et al., 2015; Gao, 2006). The Green Leaf Index (GLI) was calculated to assess changes in the vegetation cover between and within cadaver and control sites, by showing positive index values for vegetation and negative values for soil and non-vegetated areas (L3 Harris Geospatial documentation center, 2022; Lim Soon et al., 2019; Louhaichi et al., 2001).

Table 3: Overview of the vegetation indices and their formulas.

Vegetation index	Calculation	References
MGRVI	$(Green^2 – Red^2) / (Green^2 + Red^2)$	(Bendig et al., 2015)
RGBVI	$Green^2$ - (Red * Blue) / $Green^2$ + (Red * Blue)	(Bendig et al., 2015)
GLI	$(2 \cdot Green – Red – Blue) / (2 \cdot Green + Red + Blue)$	(L3 Harris Geospatial documentation center, 2022; Louhaichi et al., 2001)

The vegetation indices were also parted in new (2021) and old (2017, 2019 and 2020) sites, due to the skewed distribution in the number of cadavers and the ability to see changes over time. I chose to perform a paired Wilcoxon Signed Rank Test for new and old sites for all three vegetation indices at all three altitudes (30 m, 50 m, 100 m). This were performed to compare cadaver and control sites, both for the whole grid and the parts core, inner and outer, with the reflectance as response variable and type of site as explanatory variable.

3 Results

A total of 66 sites consisting of both a cadaver (N = 33) and a paired control plot (N = 33), were assessed by ground surveys in parallel with a drone survey. Within the 33 cadaver sites, eight of the sites originated from 2021. Three sites were from 2020, 20 sites were from 2019, and two sites were from 2017.

3.1 Vegetation survey data

3.1.1 Overall effects

The overall cadaver effect varied among the defined vegetation groups. Graminoid cover was higher at cadaver sites compared to control sites (mean Cad = 17.07, mean Con = 15.00, p-value = 0.007). Percentage cover of herbs did not differ between the cadaver and control sites (mean Cad = 15.17 %, mean Con = 15.34 %, p-value = 0.644), nor did it for woody plants (mean Cad = 11.90 %, mean Con = 12,79 %, p-value = 0.472). Lichen and bryophyte cover were lower at cadaver sites compared to control sites (lichen; mean Cad = 7.76 %, mean Con = 10.17 %, p-value = 0.066, bryophytes; mean Cad = 21.72 %, mean Con = 26.72 %, p-value = 0.004) (Figure 5, Appendix 1).

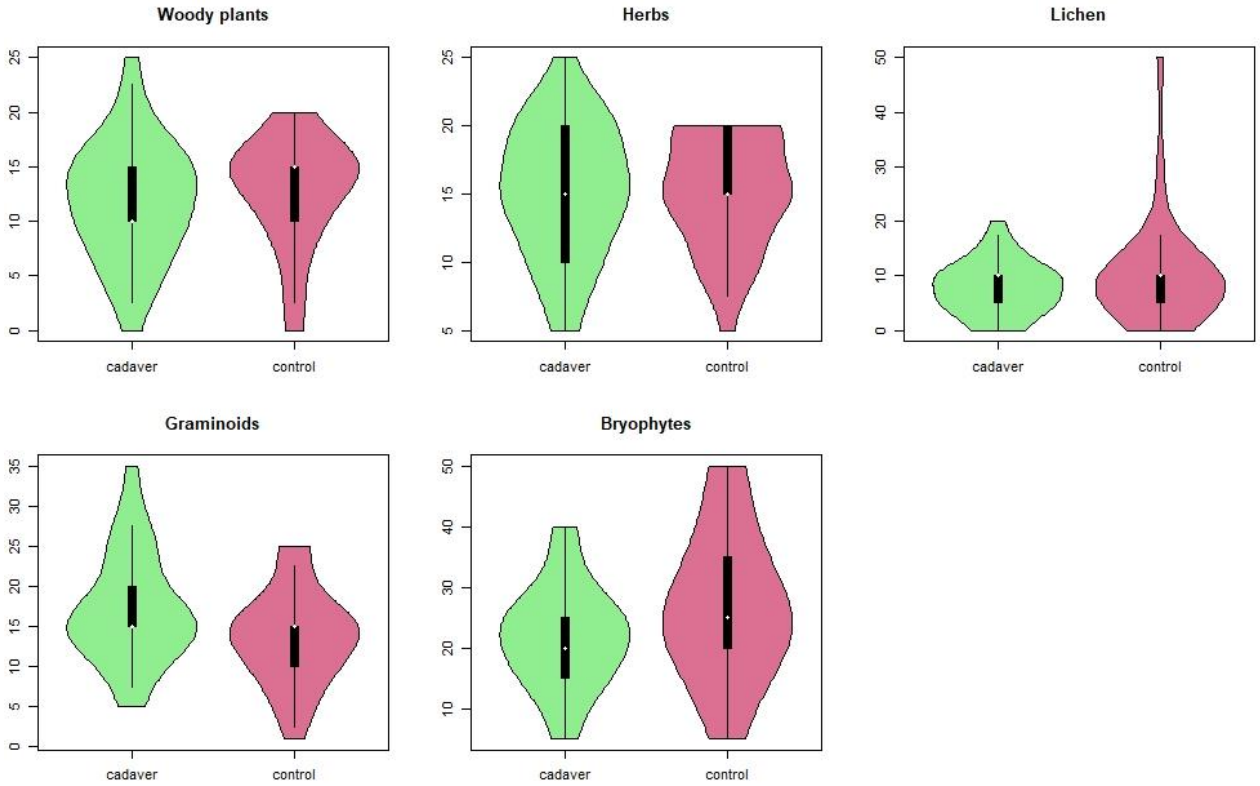

Figure 5: Observed cover of each vegetation group. Cadaver sites are represented in green, while control sites are represented in red. The white dot represents the median in each vegetation group, while the black bar shows the interquartile range.

3.1.2 Woody plants

For new cadavers, the type only model was considered as the best model (ΔAICc = 0.00, AICcWt = 0.745) (Appendix 2). This model showed that cadaver sites had a higher percentage cover of woody plants compared to the control sites (Table 5 & Figure 6).

For old cadavers, the interaction model was considered as the best fitted model (ΔAICc =0.00, AICcWt = 0.673) (Appendix 2). This model indicated the percentage cover of woody plants were significantly lower at the core of the grid of cadaver sites compared to the control sites (Table 5 & Figure 6). For the two outer bands of the grid at cadaver sites the cover was similar to the control sites.

Table 4: The type only model was the best model to explain cover of woody plants at cadaver and control sites.

Variable	Estimate	Standard Error	P-value
Intercept	-1.664	0.059	< 0.001
Type control	-0.161	0.055	0.003

Table 5: The interaction model was the best model to explain cover of woody plants at cadaver and control sites.

Variable	Estimate	Standard Error	P-value
Intercept	-2.650	0.216	< 0.001
Control site	0.499	0.202	0.014
Outer band	0.436	0.155	0.005
Inner band	0.539	0.158	0.001
Control:outer	-0.379	0.208	0.068
Control:inner	-0.487	0.212	0.022

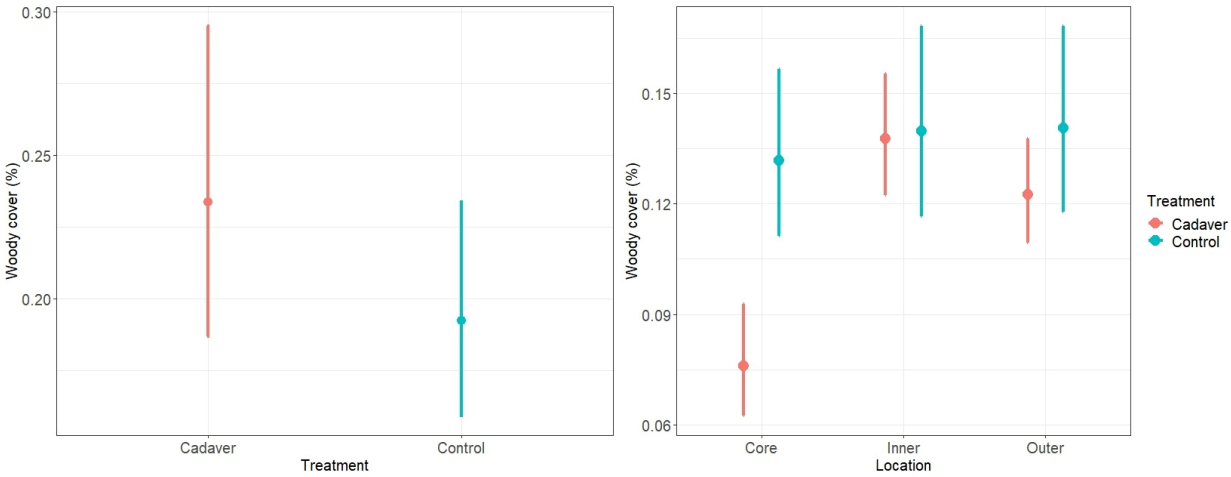

Figure 6: Show the type only model for woody plants for the new cadaver and control sites (left plot), and the interaction model for woody plants for old cadaver and control sites (right plot).

3.1.3 Graminoids

Model selection for graminoid cover at the new cadaver and control sites showed that the type only model was the best model for the data (ΔAICc =0.00, AICcWt = 0.843) (Appendix 2). The type only model showed a higher percentage cover of graminoids at cadaver sites compared to control sites (Table 6 & Figure 7).

The model selection for the old cadaver and control sites showed that the interaction model was the best fit (ΔAICc = 0.00, AICcWt = 1) (Appendix 2). The interaction model shows a clear increase in cover from the outer parts of the grid and towards the core at cadaver sites (Table 7 & Figure 7). The control sites show an overall lower percentage cover, and an even distribution throughout the grid (Figure 7).

Table 6: The type only model was the best model to explain cover of graminoids at cadaver and control sites.

Variable	Estimate	Standard Error	P-value
Intercept	-1.841	0.09500	< 0.001
Type control	-0.308	0.04462	< 0.001

Table 7: The interaction model was the best model to explain cover of graminoids at cadaver and control sites.

Variable	Estimate	Standard Error	P-value
Intercept	-6.161	0.100	< 0.001
Control site	-0.414	0.090	< 0.001
Outer band	-0.370	0.059	< 0.001
Inner band	-0.181	0.061	0.003
Control:outer	0.348	0.093	< 0.001
Control:inner	0.208	0.095	0.029

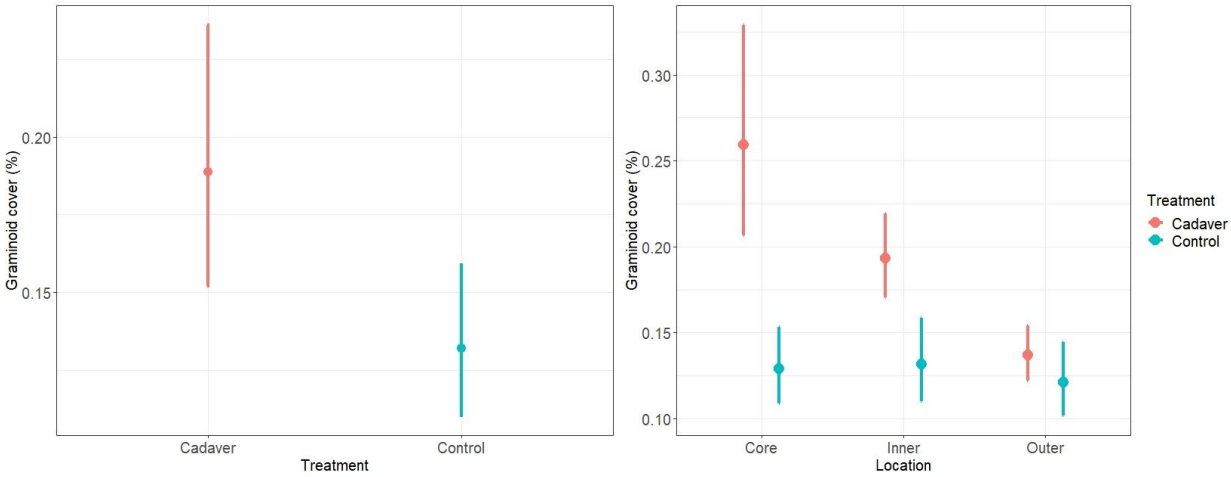

Figure 7: Show the type only model for graminoids for the new cadaver and control sites (left plot) and the interaction model for graminoids for old cadaver and control sites (right plot).

3.1.4 Herbs

The model selection for herbs for the new sites showed that the interaction model performed best (ΔAICc = 0.00, AICcWt = 0.890) (Appendix 2). This model showed a clear decrease in percentage cover of herbs from the outer parts of the grid towards the core (Table 8 & Figure 8). The cover is overall higher at control sites (Figure 8).

For the old sites, model selection indicated that the type only model was the best possible model out of the candidate models (ΔAICc = 0.00, AICcWt = 0.255) (Appendix 2). The band only model showed no significant difference between cadaver and control (Table 9 Figure 8).

Table 8: The interaction model was the best model to explain cover of herbs at cadaver and control sites.

Variable	Estimate	Standard Error	P-value
Intercept	-2.163	0.206	< 0.001
Control site	0.743	0.231	0.001
Outer band	0.451	0.185	0.015
Inner band	0.259	0.190	0.172
Control:outer	-0.537	0.238	0.023
Control:inner	-0.299	0.243	0.220

Table 9: The type only model was the best model to explain cover of herbs at cadaver and control sites.

Variable	Estimate	Standard Error	P-value
Intercept	-1.802	0.150	< 0.001
Type control	-0.021	0.030	0.488

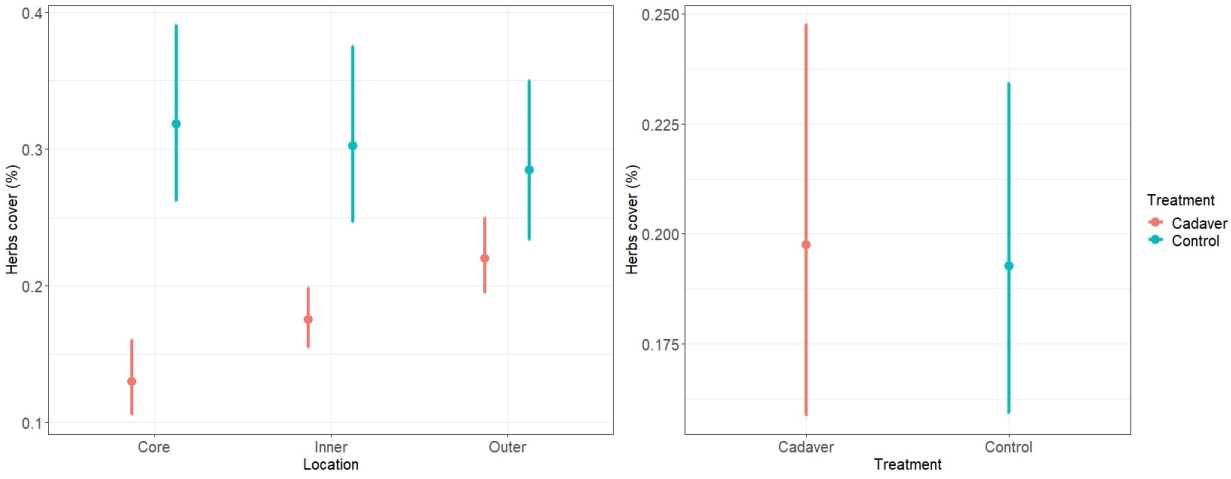

Figure 8: Show the interaction model for herbs for the new cadaver and control sites (left plot), and the type only model for herbs for old cadaver and control sites (right plot).

3.1.5 Bryophytes

For bryophytes the interaction model was the best performing model for both old and new sites (New sites: ΔAICc = 00.0, AICcWt = 0.977, Old sites: ΔAICc = 0.00, AICcWt = 1) (Appendix 2). For both old and new cadaver sites there was a clear decrease in cover of bryophytes from the outer band of the grid towards the core (Table 10 & 11, Figure 9). The percentage cover was overall higher at control sites (Figure 9).

Table 10: The interaction model was the best model to explain cover of bryophytes at cadaver and control sites.

Variable	Estimate	Standard Error	P-value
Intercept	-1.707	0.253	< 0.001
Control site	0.635	0.251	0.011
Outer band	0.583	0.194	0.003
Inner band	0.332	0.199	0.097
Control:outer	-0.624	0.258	0.016
Control:inner	-0.329	0.265	0.215

Table 11: The interaction model was the best model to explain cover of bryophytes at cadaver and control sites.

Variable	Estimate	Standard Error	P-value
Intercept	-6.62281	0.13174	< 0.001
Control site	0.53203	0.10015	< 0.001
Outer band	0.55972	0.08039	< 0.001
Inner band	0.35194	0.08241	< 0.001
Control:outer	-0.44450	0.10232	< 0.001
Control:inner	-0.26767	0.10500	0.011

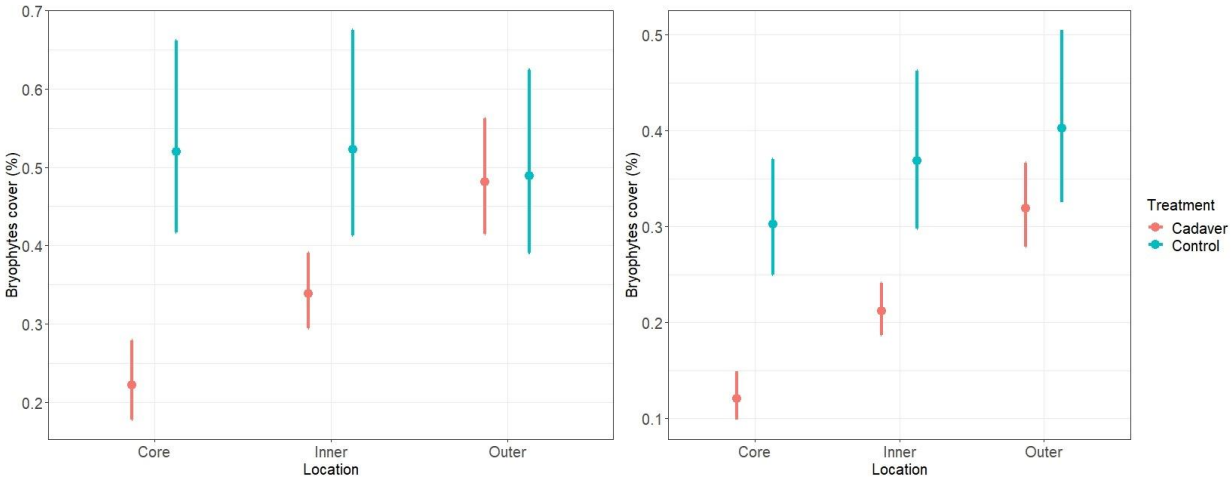

Figure 9: Show the interaction model for bryophytes for the new cadaver and control sites (left plot), and the interaction model for bryophytes for old cadaver and control sites (right plot).

3.1.6 Lichen

For lichen, interaction model performed best for both old and new sites (New sites: ΔAICc = 0.00, AICcWt = 0.695, Old sites: ΔAICc = 0.00, AICcWt = 1) (Appendix 2). Both interaction

models showed a clear decrease in percentage cover of lichen from the outer parts of the grid towards the core at cadaver sites (Table 12 & 13, Figure 10). The control sites showed an overall larger percentage cover in all parts of the grid (Figure 10).

Table 12: The interaction model was the best model to explain cover of lichen at cadaver and control sites.

Variable	Estimate	Standard Error	P-value
Intercept	-3.330	0.333	< 0.001
Control site	1.080	0.391	0.006
Outer band	0.964	0.317	0.002
Inner band	0.807	0.323	0.013
Control:outer	-0.922	0.401	0.022
Control:inner	-0.750	0.409	0.067

Table 13: The interaction model was the best model to explain cover of lichen at cadaver and control sites.

Variable	Estimate	Standard Error	P-value
Intercept	-7.386	0.126	< 0.001
Control site	0.582	0.105	< 0.001
Outer band	0.420	0.085	< 0.001
Inner band	0.308	0.087	< 0.001
Control:outer	-0.480	0.107	< 0.001
Control:inner	-0.330	0.110	0.003

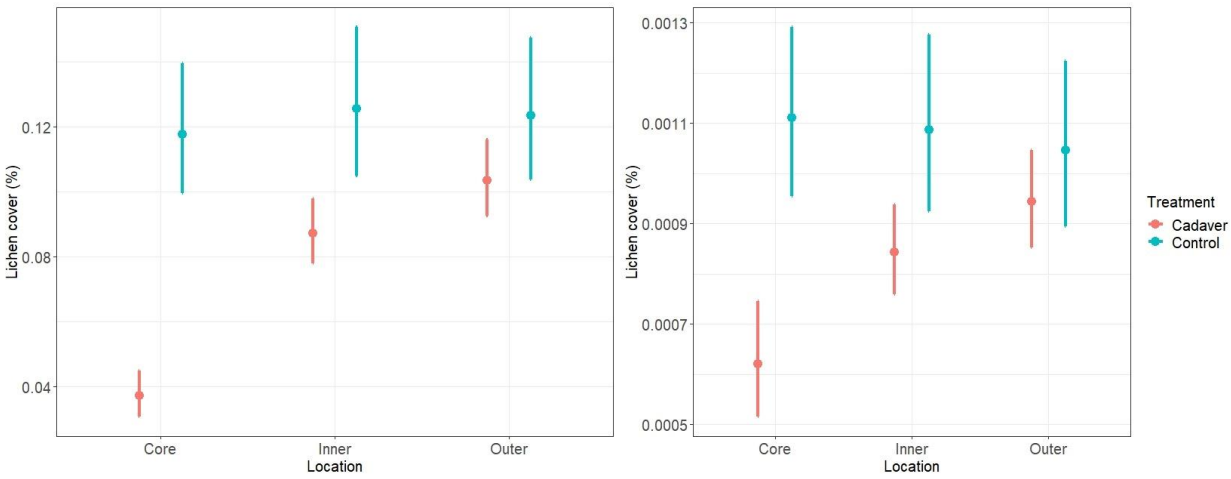

Figure 10: Show the interaction model for lichen for the new cadaver and control sites (left plot), and the interaction model for lichen for old cadaver and control sites (right plot).

3.2 Spectral indices

From the three vegetation indices the MGRVI and RGBVI had very similar results, while the GLI differs a bit from the two first ones. Because of this, I chose to focus only on MGRVI and GLI further and include the RGBVI results in the appendix (Appendix 2).

3.2.1 MRGVI

The paired Wilcoxon Signed Rank Test for the MGRVI data showed an overall pattern of higher index values at cadaver sites compared to control sites, and for all flight altitudes (30, 50, 100 m). This applies to both old and new sites pooled and for all parts of the grid.

The new sites showed a pattern of having higher index values at cadaver sites compared to control sites at 30 m altitude, but not statistically significant (Table 13 & Figure 11). For the old sites, there was a clear significant difference in higher index values at cadaver sites compared to control sites at the same altitude (Table 13).

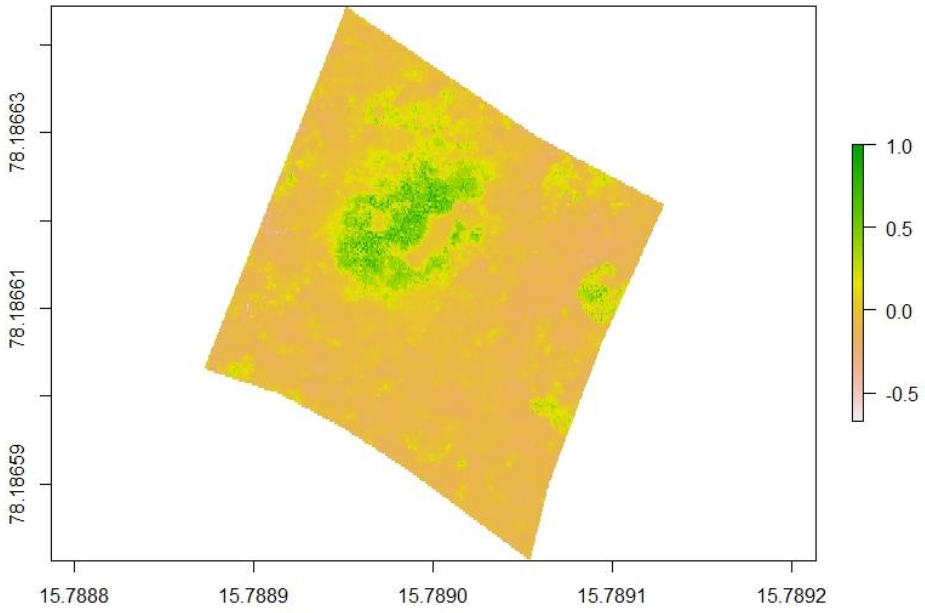

Figure 11: MGRVI image of a cadaver site from 2019 at 30m altitude. The location of the cadaver is visualized with higher values than the surroundings (green color).

At 50 m and 100m altitude there were significantly higher index values at cadaver sites compared to control sites at both old and new sites, and in the entire grid (Table 13 & Figure 12). The significance becomes clearer at the old sites, except for the outer parts of the grid (Table 13 & Figure 12).

Table 14: Results from the Wilcoxon Signed Rank Test performed for the MGRVI for both old and new sites at 30 m, 50 m, and 100 m altitude.

MGRVI (Modified Green Red Vegetation Index)		
Grid	P-value new sites	P-value old sites
Core 30 m	0.107	< 0.001
Inner 30 m	0.058	< 0.001
Outer 30 m	0.141	0.015
Total 30 m	0.107	< 0.001
Core 50 m	0.021	< 0.001
Inner 50 m	0.014	< 0.001
Outer 50 m	0.042	0.275
Total 50 m	0.021	< 0.001
Core 100 m	0.021	< 0.001
Inner 100 m	0.021	< 0.001
Outer 100 m	0.042	0.252
Total 100 m	0.030	0.003

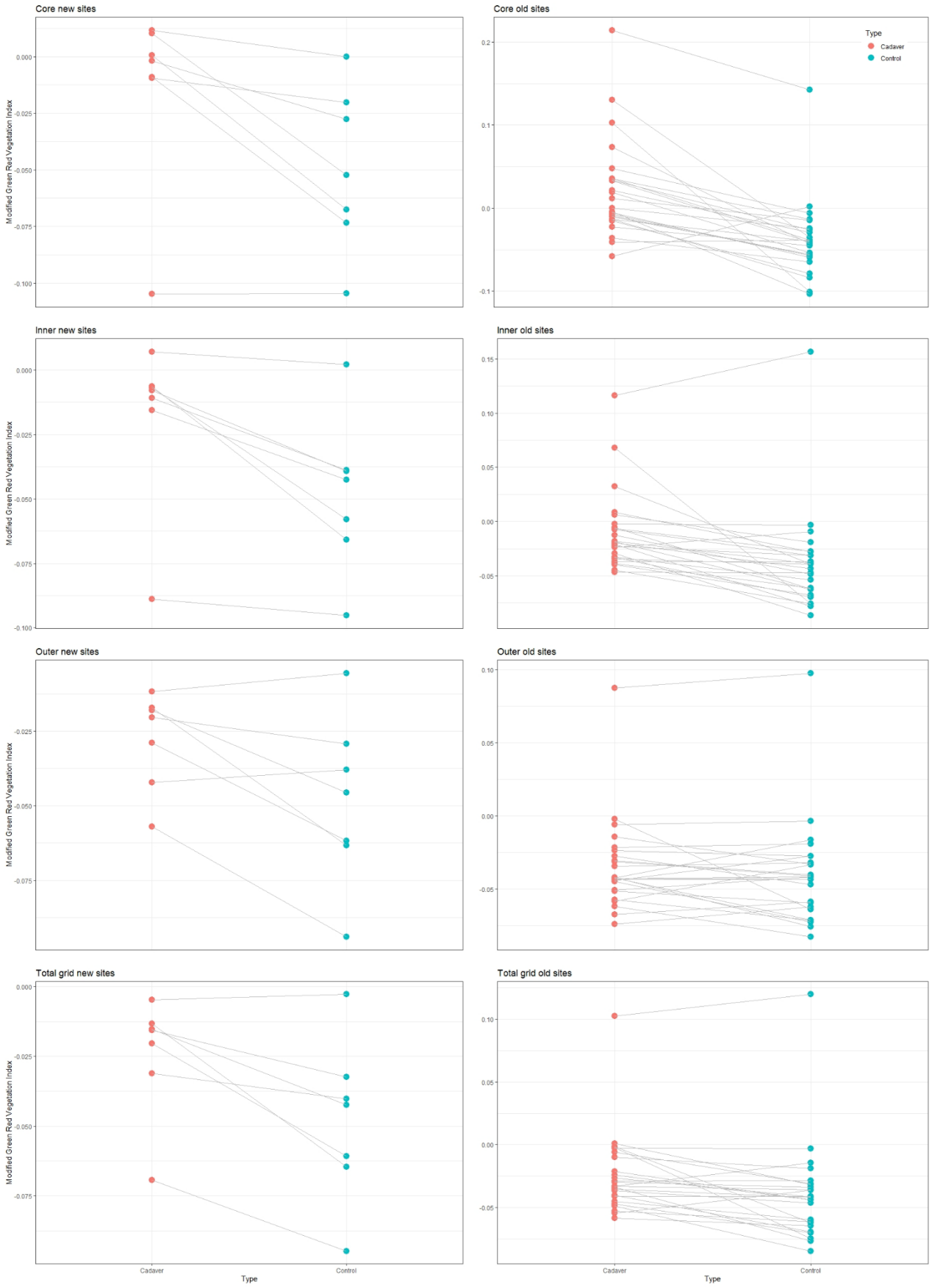

Figure 12: MGRVI values for new and old sites at 50 m altitude. The gray lines connects cadaver sites with the paired control sites.

3.2.3. GLI

The paired Wilcoxon Signed Rank Test for the GLI-data at all altitudes showed an overall pattern of lower index values at the cadaver sites compared to the control sites at the new sites. The old sites showed a pattern of higher index values at cadaver sites compared to control sites at all altitudes. This pattern was observed across all parts of the grid.

At 30 m altitude, only the inner part of the grid showed a significant pattern of lower index values at cadaver sites compared to control sites at new sites (Table 14). The core and outer part of the grid had a weaker response, which also applies for the total grid (Table 14). The old sites at 30 m altitude had significantly higher index values at cadaver sites compared to control sites in all parts of the grid, and in the entire grid as well (Table 14).

At 50 m altitude for the new sites, only the inner band of the grid had significantly lower index values compared to the control sites (Table 14 & Figure 13). The core and outer bands and the total grid showed a tendency of having lower index values at cadaver compared to control sites (Table 14 & Figure 13). For the old sites at 50 m altitude, the patterns were much clearer. The core and inner parts of the grid and the entire grid showed significantly higher index values at cadaver sites compared to control sites (Table 14 & figure 13). The outer band showed no significant difference between cadaver sites and control sites (Table 14 & Figure 13).

At 100 m altitude, for the new sites only the inner band of the grid showed significantly lower index values at cadaver sites compared to the control sites (Table 14). The rest of the grid still showed a tendency of lower index values at cadaver sites compared to control sites (Table 14). The old sites at 100 m altitude, showed significantly higher index values at the core and inner bands, in addition to the entire grid, at cadaver sites compared to the control sites (Table 14). The outer band showed no significant difference between cadaver sites and control sites (Table 14).

Table 15: Results from the Wilcoxon Signed Rank Test performed for the GLI index for both old and new sites at 30 m, 50 m, and 100 m altitude.

GLI (Green Leaf Index)		
Grid	P-value new sites	P-value old sites
Core 30 m	0.195	0.001
Inner 30 m	0.039	< 0.001
Outer 30 m	0.313	0.096
Total 30 m	0.141	0.006
Core 50 m	0.195	0.003
Inner 50 m	0.039	0.001
Outer 50 m	0.313	0.353
Total 50 m	0.080	0.048
Core 100 m	0.016	0.009
Inner 100 m	0.016	< 0.001
Outer 100 m	0.109	0.127
Total 100 m	0.233	0.004

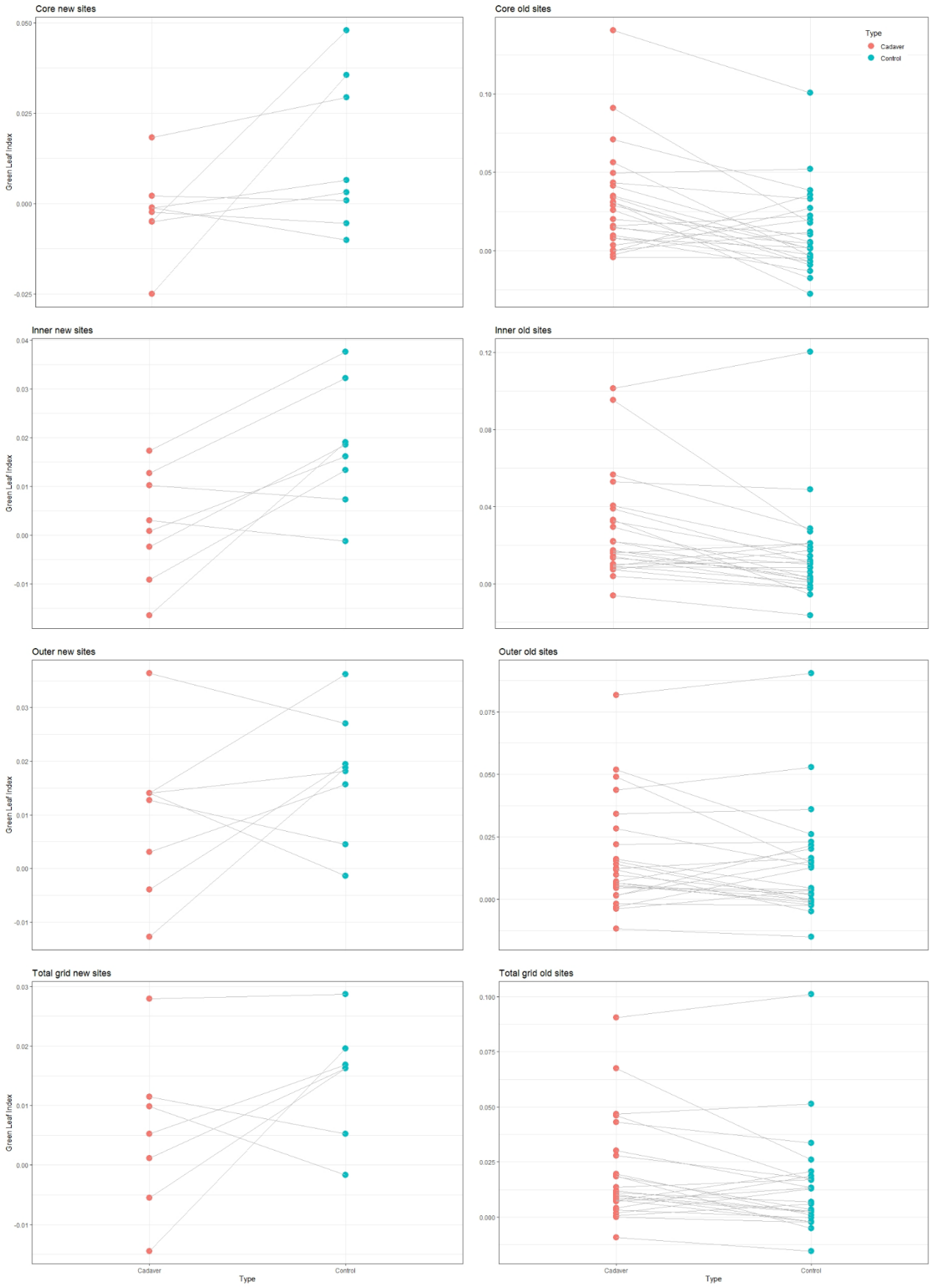

Figure 13: GLI values for new and old sites at 50 m altitude. The gray lines connects cadaver sites with the paired control sites.

4 Discussion

4.1 Cadaver impacts on the vegetation groups

By performing the ground survey in this study, the aim was to assess changes in the vegetation groups between cadaver sites and control sites. The overall response of graminoids showed a significantly higher cover and bryophytes showed a significantly lower cover at cadaver sites compared to control sites, as expected. For the remaining vegetation groups there were no significant difference between cadaver sites and control sites, contrary to the expectations. On the detailed level, graminoids showed higher cover at cadaver sites compared to paired control sites, as expected. Bryophytes and lichens showed lower cover at cadaver sites compared to paired control sites as expected. Woody plants and herbs did not, contrary to the expectations, show as clear a pattern of higher cover at cadaver sites compared to paired control sites.

Across all vegetation groups the disturbance of the cadaver seemed to constitute a gradient from the cadaver and towards the edge of the grid, which is also supported by other studies (Danell et al., 2002; Towne, 2000). Danell et al. (2002) showed a significantly higher nitrogen concentration in the plants one meter from the cadaver compared to two meter from the cadaver in their study on Muskox (*Ovibos moschatus*) cadavers in the arctic tundra of Canada, and that the vegetation was more lush close to the cadaver (Danell et al., 2002). Furthermore, a one meter gradient from the cadaver was observed where both nitrogen content and lush vegetation had faded (Danell et al., 2002). Nutrient elevation due to carcass decomposition has also been demonstrated to be persistent over time, and eight times higher levels of phosphorus in the soil at cadaver sites compared to control sites after five years of decomposition of kangaroo (*Macropus giganteus*) cadavers in grassy woodland of Canberra, Australia (Barton et al., 2016). In this case the other nutrient levels were equal at cadaver and control sites (Barton et al., 2016). Elevated phosphor levels over a long time can be explained by the slow phosphor turnover in the ecosystem, or due to continued leakage from bones and other recalcitrant remains at the cadaver sites (Barton et al., 2016). Phosphorous are also less soluble and often needs microorganisms or fungi to make it accessible to the vegetation (Rolewicz et al., 2018). At arctic sites nutrient turnover through decomposition is demonstrated lower (Danell et al., 2002).

Woody plants have been shown to react positively and increase in growth as a result of nitrogen supply, however, over time they seem to decrease in growth (Fremstad, 1992). The woody plants included in my study showed higher cover at the cadaver sites in the first

growth season compared to the control sites, corroborating earlier findings (Fremstad, 1992). After the first growth season this group showed lower cover at the core of the cadaver sites. Increased amounts of nitrogen is stated in an earlier study of nitrogen addition in High Arctic heath on Svalbard to have negative impact of woody plants (Street et al., 2015). The cover in the outer parts of the grid of the cadaver sites seem to remain relatively stable over time, more or less equal to the control sites, demonstrating that the cadaver effects reached maximum three meters. An earlier study of ungulate cadavers in the prairie of Kansas, USA, showed, however, that woody plants were not affected by cadaver decomposition (Towne, 2000). It may appear that increased supply of nutrients results in higher cover in the first growing season, but that it has a somewhat negative to no effect over time (Fremstad, 1992; Street et al., 2015; Towne, 2000).

Graminoids shows a tendency of increasing in growth with increasing nitrogen supply (Fremstad, 1992). My results confirmed this pattern and graminoids showed higher percentage cover at the cadaver sites compared to the control sites in the first growing season. This is consistent with a study done on Zebra (*Equus quagga*) cadavers in semi-arid savannah in Namibia, South-Africa, where the researchers found significantly higher biomass of grasses at cadaver sites compared to control sites the first year after the zebra`s death (Turner et al., 2014). After the first growing season the high cover of graminoids in my study persisted, especially at the core but also in the inner and outer band of the grid. The control sites had an overall lower graminoid cover. In addition to the known benefit from nitrogen supply graminoids have also showed this type of response at cadaver sites in earlier studies (Barton et al., 2013; Towne, 2000; Turner et al., 2014). Barton et al. (2016) in fact stated that cadaver sites favored grasses. Under cool conditions, high levels of nitrogen are known to favor graminoids (Towne, 2000), which may explain some of the increased grass growth in the Arctic tundra. This increase in graminoid cover usually happen at the expense of other vegetation groups (Fremstad, 1992). Here, I demonstrated that cadaver decomposition within Arctic tundra has a positive effect on graminoid cover, and that the response comes first around the cadaver center and spreads over time.

Herbs have earlier show to increase in growth for low levels of nitrogen addition, but a decrease with high levels of nitrogen addition (Fremstad, 1992). My results showed that the herbs had lower cover at the outer band towards the core of the cadaver sites in the first growing season. In the study from Bump et al. (2009) on white-tailed deer (*Odocoileus virginianu*) cadavers in hardwood forest in Michigan, USA, a decrease in herbaceous species

the two first growth seasons was observed, with the largest decrease in the first growth season. Within older sites the response to the cadaver decomposition seemed to fade and was less pronounced (Bump et al., 2009). An even response across smaller spatial scales within the older cadaver sites is supported by Towne`s study (2000) of ungulate cadavers in the prairie of Kansas, USA. Contrary to my results, he found a decrease in the cover of herbs in the cadaver center followed by a significant increase in the same area after three years (Towne, 2000). Street et al. (2015) showed that vascular plants responded by decreasing in prevalence, and sometimes even complete mortality as a result of nutrient addition in arctic tundra. This response had faded after 22 years (Street et al., 2015). The cadaver decomposition can thus seem to have highest negative impact on herbs the first growing seasons, although it is known to persist over time (Bump et al., 2009; Fremstad, 1992; Street et al., 2015; Towne, 2000). An important notion when mapping herbs in a percentage cover method is that they are usually not very space consuming, especially within arctic areas (Billings, 1974), and can therefore experience some kind of mapping bias when using this approach.

Small amounts of nitrogen supply initially lead to increased lichen growth, but it can also lead to greater competition on light access and space (Johansson et al., 2012; Street et al., 2015). Slow growing species, like most lichens and bryophytes, will thus probably be outcompeted when the nitrogen supply increases (Johansson et al., 2012; Street et al., 2015). Input of low amounts of nitrogen increased overall lichen growth over a four-year time-span in spruce forests in Sweden (Johansson et al., 2012). However large amounts of nitrogen input decreased the overall growth of lichens within the same habitat (Johansson et al., 2012). The lichen community is one of the most sensitive communities when it comes to changes in nitrogen supply (Johansson et al., 2012). Increased nitrogen concentration in the lichen thallus may adversely affect stability and the chemical defense mechanism of the lichen (Johansson et al., 2012). This can lead to the lichen being more easily exposed to parasite attacks, and more easily fragmented by, for example, strong winds (Johansson et al., 2012). Both of these aspects will lead to lower biomass. Lichen cover immediately decrease when high amounts of nitrogen is added, and in combination with phosphorus this decrease aggravates, and persists for long time periods (Street et al., 2015). My results showed an immediate lower cover of lichen at cadaver sites that lasted throughout the time-frames of this study, thus underpinning lichens as a sensitive group strongly affected by nutrient elevation. I found a clear pattern of lowest cover of lichen in the core of the cadaver sites that faded towards the border of the

grid. My results on cadaver effects on lichen are thus in line with several studies showing that cadaver decomposition and high levels of nutrient supply has a negative effect on lichen cover (Johansson et al., 2012; Street et al., 2015).

Bryophytes have previously been shown to significantly decrease through nitrogen addition, and may be sensitive to high amounts of the element (Fremstad, 1992). Street et al. (2015) discovered in contrast an increase in bryophyte cover as a result of nutrient supply. Both nitrogen and phosphorus gave a positive response that still persisted 22 years after the supply (Street et al., 2015). My results showed an immediate lower cover of bryophytes at cadaver sites compared to control sites. There was a clear pattern of lowest cover at the core that became smaller towards the border of the grid. Sun et al. (2017) stated in their study that the response to increased nutrient supply in bryophytes seemed to have more impact on species and ecosystem levels, rather than as a functional group. The bryophytes can thus seem to respond both positive and negative on nutrient supply and cadaver decomposition depending on species present and place of growth (Fremstad, 1992; Street et al., 2015; Sun et al., 2017).

4.2 Cadaver decomposition leads to greener vegetation

The aim of calculating vegetation indices using drones with RGB camera in this study was to assess whether or not the vegetation gets affected by cadaver decomposition, and the spatial distribution of this impact. The vegetation indices MGRVI and GLI showed an increase in chlorophyll production at cadaver sites, while the new cadaver sites showed less vegetation compared to control sites, as expected. The vegetation at cadaver sites showed significantly higher index values of MGRVI compared to control sites. This increase occurred already during the first year after the reindeer`s death and remained throughout the years of this study. At the same time the cadaver sites showed a decrease in index value of GLI and thus a lack of vegetation in the immediate surroundings of the cadaver sites compared to the control sites within the first growing season after the reindeer`s death. For the following years an upheaval occurred, and the cadaver sites showed an increase in index value of GLI and a greening of vegetation, in the center of the grid.

The vegetation index MGRVI was used to detect variation in chlorophyll absorption in vegetation, and the results showed significantly higher index values at cadaver sites compared to control sites, indicating higher chlorophyll absorption and productivity in the vegetation (Barbosa et al., 2019; Bendig et al., 2015). The higher index values at cadaver sites compared to control sites did not differ between old and new sites. It may therefore be reasonable to

believe that chlorophyll absorption increased immediately with the first nutrients added to the environment from the cadaver decomposition. This corresponds to the study by Barton et al. (2013) who discovered a large increase of nitrogen in both soil and plants just a few weeks after the cadaver started to decompose. Also, Turner et al. (2014) found significantly higher nitrogen content in the grasses at cadaver sites compared to control sites. High nitrogen content in the vegetation at cadaver sites compared to control sites indicates higher photosynthetic potential (Bump et al., 2009). Other studies found a large degree of elevated content of nitrogen, nitrate, and phosphorus in the soil under the cadaver that decreased with increasing distance from the cadaver, both the in first growing season and after three years (Bump et al., 2009; Towne, 2000). My results of high index values of MGRVI corroborating previous findings that the cadaver center becomes a nutrient hotspot and leads to vegetation biomass increase (Carter et al., 2006; Newsome et al., 2021; Towne, 2000; Turner et al., 2014).

The GLI was calculated to assess if the presence of the cadavers provided an effect on the presence of the vegetation. This index was chosen because it provided good results for identifying exposed soil or lack of vegetation in earlier studies (Barbosa et al., 2019). The new sites showed a clear decrease in GLI index values at cadaver sites compared to control sites, with a clear pattern of lower index values in the core and inner parts of the grid. The outer parts of the grid were not affected equally. The low index values suggested less vegetation in the core and inner parts of the grid due to the cadaver during the first growth season. For the new cadaver sites, large amount of cadaver remains were still present. These cadaver remains covered the vegetation and occupied space from, shaded out, and suffocated the vegetation (Barton et al., 2013; Carter et al., 2006). The nutrient flow from the cadaver may also become too concentrated for the vegetation to cope with (Carter et al., 2006).

For the old sites, the reflectance pattern looked completely different. The core and inner parts of the grid showed an increased reflectance at cadaver sites compared to the control sites. The outer part of the grid, equal to the new sites, did not show the same effect. After the first growth season the cadaver decomposition seemed to be beneficial to the vegetation. This corresponds to an earlier study on biomass estimation in grasslands, where the GLI showed increasing reflectance with increasing nitrogen supply (Lussem et al., 2018). At this point the cadavers were largely decomposed and did not occupy a lot of space. At this point the vegetation also has had time to absorb nutrients derived from the cadaver. Some parts of the cadaver such as bone, hair, and hooves can take many years to decompose, and will supply

the surroundings with phosphorous and calcium for a long time after the reindeer`s death (Barton et al., 2019; Newsome et al., 2021).

4.3 Cadaver decomposition in the Arctic tundra ecosystem

On the ecosystem level, cadaver decomposition can make a great disturbance (Carter et al., 2006). Because the nutrient turnover in the Arctic tundra is low (Danell et al., 2002; Jonasson & Shaver, 1999) a disturbance from a cadaver could remain for a long time (Street et al., 2015). The cadaver decomposition may lead to especially green patches in the landscape (Carter et al., 2006; Newsome et al., 2021), and thus increase the diversity in the landscape (Barton et al., 2019; Bump et al., 2009). Since my study only looked at cadavers up to four years after death, and Danell et al. (2002) stated an effect still after 10 years, an interesting question to ask will be how long it takes before and if the tundra returns to its original state after such a disturbance.

4.4 Sources of error

The “new sites” category contains of a smaller sample size than the “old sites” category and this should be kept in mind when interpreting the results. Within the 33 cadaver sites and 33 control sites (66 in total), eight of the cadaver and control sites are from 2021 constituting the category “new sites”. The remaining 25 cadaver and control sites spanned three years: 2020 (three sites), 2019 (20 sites), 2017 (two sites), constituting the category “old sites”. There is thus a potential bias within the data, due to uneven distribution of sites across years and categories.

Calculation of vegetation indices from RGB images has previously shown a weakness with reporting falsely high values on images strongly affected by sunlight (Barbosa et al., 2019). Different solar conditions of different field days may thus create sources of error in the results (Barbosa et al., 2019; Rasmussen et al., 2016), but the paired cadaver and control plots were flown at same time and should therefore not be affected to a large extent. Rasmussen et al. (2016) states that the shadows and sources of error in the images becomes larger when the elevation angle of the sun becomes lower. It is therefore plausible to assume that the images in this study should have a rather small degree of influence, as Svalbard has midnight sun and the sun in a high elevation angel during summertime when the data collection were performed. During the field work, it was also almost constantly cloudy, which gives very stable conditions.

Another aspect to consider in the interpretation of the results is that the number of squares in the three bands of the grid is different. The data for the core is based on only one square, while the outer band consists of data from sixteen squares. The inner band consists of eight squares. It therefore requires less change to get major effects in the core than for example the outer band.

5.0 Conclusion

Cadaver decomposition affects vegetation cover and have different effects across functional groups. Graminoids showed an unambiguous increase in prevalence due to nutrient supply by cadaver decomposition across space and time. Bryophytes and lichen showed an unambiguous decrease in prevalence due to increased nutrient supply through cadaver decomposition, in both space and time. Woody plants showed an early positive response on nutrient supply from cadaver decomposition, while herbs showed a negative response to the nutrient supply from cadaver decomposition. In the arctic tundra where the nutrient turnover is especially slow (Danell et al., 2002; Jonasson & Shaver, 1999), the effect of disturbance in terms of nutrient supply may remain a factor for a long time (Street et al., 2015). The vegetation in cold areas is also exposed to greater stress and even small disturbances or the addition of nutrients in small quantities could thus create a great impact on the ecosystem (Fremstad, 1992).

Drones and calculation of vegetation indices from drone images can be used in, among others, studies of forage quality, nitrogen content in rice leaf, forestry and vegetation index reflection of corn and sugar beets (Astor et al., 2020; Li et al., 2018; Olson et al., 2019; Torresan et al., 2017). The calculation of MGRVI showed that the vegetation increases chlorophyll absorption immediately by the supply of nutrients from cadaver decomposition, and that this remains for at least the four years covered in my study. The GLI, on the other hand, showed a decrease in reflection and absence of vegetation in the first year after the reindeer`s death, but a significant increase occurs after the first year. The high reflectance of MGRVI in also the first year suggests that chlorophyll absorption increases already from the first supply of nutrients. The clear results from this study, corroborating earlier findings (Barbosa et al., 2019; Lussem et al., 2018; Olson et al., 2019), justifies the usage of drones in research as an effective and good method for detecting vegetation changes.

6 Literature

Agisoft. (2022). *Agisoft*. https://www.agisoft.com/

Astor, T., Schulze-Brüninghoff, D., Wengert, M., & Wachendorf, M. (2020). Predicting Forage Quality of Grasslands Using UAV-Borne Imaging Spectroscopy. *Remote sensing (Basel, Switzerland)*, *12*(1), 126. https://doi.org/10.3390/rs12010126

Barbosa, B. D. S., Ferraz, G. A. S., Gonçalves, L. M., Marin, D. B., Maciel, D. T., Ferraz, P. F. P., & Rossi, G. (2019). RGB vegetation indices applied to grass monitoring: a qualitative analysis. *Agronomy Research*. https://doi.org/10.15159/AR.19.119

Bareth, G., Bareth, G., Bolten, A., Bolten, A., Gnyp, M. L., Reusch, S., & Jasper, J. (2016). Comparison of uncalibrated RGBVI with spectrometer-based NDVI derived from UAV sensing systems on field scale. *International archives of the photogrammetry, remote sensing and spatial information sciences.*, *XLI-B8*, 837-843. https://doi.org/10.5194/isprs-archives-XLI-B8-837-2016

Barton, P. S., Cunningham, S. A., Lindenmayer, D. B., & Manning, A. D. (2012). The role of carrion in maintaining biodiversity and ecological processes in terrestrial ecosystems. *Oecologia*, *171*(4), 761-772. https://doi.org/10.1007/s00442-012-2460-3

Barton, P. S., Cunningham, S. A., Macdonald, B. C. T., McIntyre, S., Lindenmayer, D. B., & Manning, A. D. (2013). Species Traits Predict Assemblage Dynamics at Ephemeral Resource Patches Created by Carrion. *PLoS One*, *8*(1), e53961-e53961. https://doi.org/10.1371/journal.pone.0053961

Barton, P. S., Evans, M. J., Foster, C. N., Pechal, J. L., Bump, J. K., Quaggiotto, M. M., & Benbow, M. E. (2019). Towards Quantifying Carrion Biomass in Ecosystems. *Trends Ecol Evol*, *34*(10), 950-961. https://doi.org/10.1016/j.tree.2019.06.001

Barton, P. S., McIntyre, S., Evans, M. J., Bump, J. K., Cunningham, S. A., & Manning, A. D. (2016). Substantial long‐term effects of carcass addition on soil and plants in a grassy eucalypt woodland. *Ecosphere (Washington, D.C)*, *7*(10), n/a. https://doi.org/10.1002/ecs2.1537

Bendig, J., Yu, K., Aasen, H., Bolten, A., Bennertz, S., Broscheit, J., Gnyp, M. L., & Bareth, G. (2015). Combining UAV-based plant height from crop surface models, visible, and near infrared vegetation indices for biomass monitoring in barley. *International journal of applied earth observation and geoinformation*.

Billings, W. D. (1974). *Arctic and Alpine vegetation: plant adaptations to cold summer climates*.

Blaalid, R., Davey, M. L., Kauserud, H., Carlsen, T., Halvorsen, R., Høiland, K., & Eidesen, P. B. (2014). Arctic root-associated fungal community composition reflects environmental filtering. *Mol Ecol*, *23*(3), 649-659. https://doi.org/10.1111/mec.12622

Bump, J. K., Webster, C. R., Vucetich, J. A., Peterson, R. O., Shields, J. M., & Powers, M. D. (2009). Ungulate Carcasses Perforate Ecological Filters and Create Biogeochemical Hotspots in Forest Herbaceous Layers Allowing Trees a Competitive Advantage. *Ecosystems (New York)*, *12*(6), 996-1007. https://doi.org/10.1007/S10021-009-9274-0

Carter, D. O., Yellowlees, D., & Tibbett, M. (2006). Cadaver decomposition in terrestrial ecosystems. *Naturwissenschaften*, *94*(1), 12-24. https://doi.org/10.1007/s00114-006-0159-1

Corder, G. W., & Foreman, D. I. (2014). *Nonparametric statistics : a step-by-step approach* (Second edition. ed.). Wiley.

Curran, P. J., & Williamson, H. D. (1987). Estimating the Green Leaf Area Index of Grassland with Airborne Multispectral Scanner Data. *Oikos*, *49*(2), 141-148. https://doi.org/10.2307/3566019

Danell, K., Berteaux, D., & Brathen, K. A. (2002). Effect of Muskox Carcasses on Nitrogen Concentration in Tundra Vegetation. *Arctic*, *55*(4), 389-392. https://doi.org/10.14430/arctic723

De Swaef, T., Maes, W. H., Aper, J., Baert, J., Cougnon, M., Reheul, D., Steppe, K., Roldan-Ruiz, I., & Lootens, P. (2021). Applying RGB- and Thermal-Based Vegetation Indices from UAVs for High-Throughput Field Phenotyping of Drought Tolerance in Forage Grasses. *Remote sensing (Basel, Switzerland)*, *13*(1), 147. https://doi.org/10.3390/rs13010147

Eischeid, I., Soininen, E. M., Assmann, J. J., Ims, R. A., Madsen, J., Pedersen, Å. Ø., Pirotti, F., Yoccoz, N. G., & Ravolainen, V. T. (2021). Disturbance Mapping in Arctic Tundra Improved by a Planning Workflow for Drone Studies: Advancing Tools for Future Ecosystem Monitoring. *Remote sensing (Basel, Switzerland)*, *13*(21), 4466. https://doi.org/10.3390/rs13214466

Esri. (2022). *ArcGIS Pro*. https://www.esri.com/en-us/arcgis/products/arcgis-pro/overview

European Union Aviation Safety Agency. (2021). *Civil drones (Unmanned aircraft)*. Retrieved 08.01.21 from https://www.easa.europa.eu/domains/civil-drones-rpas

Fremstad, E. (1992). *Virkninger av nitrogen på heivegetasjon : en litteraturstudie* (Vol. 124). Norsk institutt for naturforskning.

Gao, J. (2006). Canopy chlorophyll estimation with hyperspectral remote sensing.

Guan, S., Fukami, K., Matsunaka, H., Okami, M., Tanaka, R., Nakano, H., Sakai, T., Nakano, K., Ohdan, H., & Takahashi, K. (2019). Assessing Correlation of High-Resolution NDVI with Fertilizer Application Level and Yield of Rice and Wheat Crops using Small UAVs. *Remote sensing (Basel, Switzerland)*, *11*(2), 112. https://doi.org/10.3390/rs11020112

Hansen, B. B., Pedersen, Å. Ø., Peeters, B., Le Moullec, M., Albon, S. D., Herfindal, I., Sæther, B. E., Grøtan, V., & Aanes, R. (2019). Spatial heterogeneity in climate change effects decouples the long‐term dynamics of wild reindeer populations in the high Arctic. *Glob Chang Biol*, *25*(11), 3656-3668. https://doi.org/10.1111/gcb.14761

Johansen, B. E., Tømmervik, H., & Karlsen, S. R. (2009). *Vegetasjonskart over Svalbard basert på satellittdata : dokumentasjon av metoder og vegetasjonsbeskrivelser* (Vol. 456). Norsk institutt for naturforskning.

Johansson, O., Palmqvist, K., & Olofsson, J. (2012). Nitrogen deposition drives lichen community changes through differential species responses. *Glob Change Biol*, *18*(8), 2626-2635. https://doi.org/10.1111/j.1365-2486.2012.02723.x

Jonasson, S., & Shaver, G. R. (1999). Within-Stand Nutrient Cycling in Arctic and Boreal Wetlands. *Ecology (Durham)*, *80*(7), 2139-2150. https://doi.org/10.1890/0012-9658(1999)080[2139:WSNCIA]2.0.CO

L3 Harris Geospatial documentation center. (2022). Broadband Greenness. (14.03.22). https://www.l3harrisgeospatial.com/docs/broadbandgreenness.html#:~:text=State%20University%2C%202005.-,Green%20Leaf%20Index%20(GLI),from%20%2D1%20to%20%2B1.

Le Moullec, M., Pedersen, Å. Ø., Stien, A., Rosvold, J., & Hansen, B. B. (2019). A century of conservation: The ongoing recovery of svalbard reindeer. *The Journal of wildlife management*, *83*(8), 1676-1686. https://doi.org/10.1002/jwmg.21761

Lee, Y. K. (2020). *Arctic Plants of Svalbard : What We Learn From the Green in the Treeless White World* (1st ed. 2020. ed.). Springer International Publishing : Imprint: Springer.

Li, S., Ding, X., Kuang, Q., Ata-Ui-Karim, S. T., Cheng, T., Liu, X., Tian, Y., Zhu, Y., Cao, W., & Cao, Q. (2018). Potential of UAV-Based Active Sensing for Monitoring Rice Leaf Nitrogen Status. *Front Plant Sci*, *9*, 1834-1834. https://doi.org/10.3389/fpls.2018.01834

Lim Soon, E., Rozita, I., Wahidah, H., & Aslina, B. (2019). The Use of VARI, GLI, and VIgreen Formulas in Detecting Vegetation In aerial Images. *International Journal of Technology*, *10*(7), 1385-1394. https://doi.org/10.14716/ijtech.v10i7.3275

Louhaichi, M., Borman, M. M., & Johnson, D. E. (2001). Spatially Located Platform and Aerial Photography for Documentation of Grazing Impacts on Wheat. *Geocarto international*, *16*(1), 65-70. https://doi.org/10.1080/10106040108542184

Lussem, U., Bolten, A., Gnyp, M. L., Jasper, J., & Bareth, G. (2018). Evaluation of RGB-based vegetation indices from UAV imagery to estimate forage yield in Grassland. *International Archives of the Photogrammetry, Remote Sensing and Spatial Information Sciences - ISPRS Archives*, *42*(3), 1215-1219. https://doi.org/10.5194/isprs-archives-XLII-3-1215-2018

Magnusson, A., Skaug, H., Nielsen, A., Berg, C., Kristensen, K., Maechler, M., van Bentham, K., Bolker, B., Sadat, N., Lüdecke, D., Lenth, R., O'Brien, J., Geyer, C. J., McGillycuddy, M., & Brooks, M. (2022). *glmmTMB: Generalized Linear Mixed Models using Template Model Builder*. Retrieved 24.02.2022 from https://cran.r-project.org/web/packages/glmmTMB/index.html

Martin, A. C., Macias‐Fauria, M., Bonsall, M. B., Forbes, B. C., Zetterberg, P., & Jeffers, E. S. (2022). Common mechanisms explain nitrogen‐dependent growth of Arctic shrubs over three decades despite heterogeneous trends and declines in soil nitrogen availability. *New Phytol*, *233*(2), 670-686. https://doi.org/10.1111/nph.17529

Melis, C., Selva, N., Teurlings, I. J. M., Skarpe, C., Linnell, J. D. C., & Andersen, R. (2007). Soil and vegetation nutrient response to bison carcasses in Bialowieza Primeval Forest, Poland. *Ecological research*, *22*(5), 807-813. https://doi.org/10.1007/s11284-006-0321-4

Neumann, C., Schindhelm, A., Müller, J., Weiss, G., Liu, A., & Itzerott, S. (2021). The regenerative potential of managed calluna heathlands— revealing optical and structural traits for predicting recovery dynamics. *Remote sensing (Basel, Switzerland)*, *13*(4), 1-15. https://doi.org/10.3390/rs13040625

Newsome, T. M., Barton, B., Buck, J. C., DeBruyn, J., Spencer, E., Ripple, W. J., & Barton, P. S. (2021). Monitoring the dead as an ecosystem indicator. *Ecology and Evolution*, *11*(11), 5844-5856. https://doi.org/10.1002/ece3.7542

Nybakk, K., Kjelvik, O., Kvam, T., Overskaug, K., & Sunde, P. (2002). Mortality of semi-domestic Reindeer Rangifer tarandus in Central Norway. *Wildlife biology*, *8*(1), 63-68. https://doi.org/10.2981/wlb.2002.009

Olson, D., Chatterjee, A., Franzen, D. W., & Day, S. S. (2019). Relationship of Drone‐Based Vegetation Indices with Corn and Sugarbeet Yields. *Agronomy journal*, *111*(5), 2545-2557. https://doi.org/10.2134/agronj2019.04.0260

Parmenter, R. R., & MacMahon, J. A. (2009). Carrion Decomposition and Nutrient Cycling in a Semiarid Shrub—Steppe Ecosystem. *Ecological monographs*, *79*(4), 637-661. https://doi.org/10.1890/08-0972.1

Pettorelli, N., Vik, J. O., Mysterud, A., Gaillard, J.-M., Tucker, C. J., & Stenseth, N. C. (2005). Using the satellite-derived NDVI to assess ecological responses to environmental change. *Trends Ecol Evol*, *20*(9), 503-510. https://doi.org/10.1016/j.tree.2005.05.011

Pix4D AS. (2022). *Pix4D*. https://www.pix4d.com/

Prach, K., Walker, L. R., & Chang, C. (2019). Differences between primary and secondary plant succession among biomes of the world. *The Journal of ecology*, *107*(2), 510-516. https://doi.org/10.1111/1365-2745.13078

R Core Team. (2022). *The R Project for Statistical Computing*. Retrieved 24.02.2022 from https://www.r-project.org/

Rasmussen, J., Ntakos, G., Nielsen, J., Svensgaard, J., Poulsen, R. N., & Christensen, S. (2016). Are vegetation indices derived from consumer-grade cameras mounted on UAVs sufficiently reliable for assessing experimental plots? *European journal of agronomy*, *74*, 75-92. https://doi.org/10.1016/j.eja.2015.11.026

Reed, H. B. (1958). A Study of Dog Carcass Communities in Tennessee, with Special Reference to the Insects. *The American midland naturalist*, *59*(1), 213-245. https://doi.org/10.2307/2422385

Reimers, E. (2012). Svalbard reindeer population size and trends in four sub-areas of Edgeøya. *Polar research*, *31*(1), 11089-11085. https://doi.org/10.3402/polar.v31i0.11089

Rolewicz, M., Rusek, P., & Borowik, K. (2018). Obtaining of granular fertilizers based on ashes from combustion of waste residues and ground bones using phosphorous solubilization by bacteria Bacillus megaterium. *J Environ Manage*, *216*, 128-132. https://doi.org/10.1016/j.jenvman.2017.05.004

Rouyet, L., Lauknes, T. R., Christiansen, H. H., Strand, S. M., & Larsen, Y. (2019). Seasonal dynamics of a permafrost landscape, Adventdalen, Svalbard, investigated by InSAR. *Remote sensing of environment*, *231*, 111236. https://doi.org/10.1016/j.rse.2019.111236

Soudzilovskaia, N. A., Onipchenko, V. G., Cornelissen, J. H. C., & Aerts, R. (2005). Biomass production, N:P ratio and nutrient limitation in a Caucasian alpine tundra plant community. *Journal of vegetation science*, *16*(4), 399-406. https://doi.org/10.1111/j.1654-1103.2005.tb02379.x

Street, L. E., Burns, N. R., & Woodin, S. J. (2015). Slow recovery of High Arctic heath communities from nitrogen enrichment. *New Phytol*, *206*(2), 682-695. https://doi.org/10.1111/nph.13265

Sun, S. Q., Wang, G. X., Chang, S. X., Bhatti, J. S., Tian, W. L., Luo, J., & Halvorsen, R. (2017). Warming and nitrogen addition effects on bryophytes are species‐ and plant community‐specific on the eastern slope of the Tibetan Plateau. *Journal of vegetation science*, *28*(1), 128-138. https://doi.org/10.1111/jvs.12467

Torresan, C., Berton, A., Carotenuto, F., Di Gennaro, S. F., Gioli, B., Matese, A., Miglietta, F., Vagnoli, C., Zaldei, A., & Wallace, L. (2017). Forestry applications of UAVs in Europe: a review. *International journal of remote sensing*, *38*(8-10), 2427-2447. https://doi.org/10.1080/01431161.2016.1252477

Towne, E. G. (2000). Prairie Vegetation and Soil Nutrient Responses to Ungulate Carcasses. *Oecologia*, *122*(2), 232-239. https://doi.org/10.1007/PL00008851

Turner, W. C., Kausrud, K. L., Krishnappa, Y. S., Cromsigt, J. P. G. M., Ganz, H. H., Mapaure, I., Cloete, C. C., Havarua, Z., Küsters, M., Getz, W. M., & Stenseth, N. C. (2014). Fatal attraction: vegetation responses to nutrient inputs attract herbivores to infectious anthrax carcass sites.

Tømmervik, H., Karlsen, S.-R., Nilsen, L., Johansen, B., Storvold, R., Zmarz, A., Beck, P. S., Høgda, K. A., Goetz, S., Park, T., Zagajewski, B., Myneni, R. B., & Bjerke, J. W. (2014). Use of unmanned aircraft systems (UAS) in a multi-scale vegetation index study of arctic plant communities in Adventdalen on Svalbard. https://doi.org/10.12760/02-2014-1-09

van Klink, R., van Laar-Wiersma, J., Vorst, O., & Smit, C. (2020). Rewilding with large herbivores: Positive direct and delayed effects of carrion on plant and arthropod communities. *PLoS One*, *15*(1). https://doi.org/10.1371/journal.pone.0226946

Wan, L., Li, Y., Cen, H., Zhu, J., Yin, W., Wu, W., Zhu, H., Sun, D., Zhou, W., & He, Y. (2018). Combining UAV-Based Vegetation Indices and Image Classification to

Estimate Flower Number in Oilseed Rape. *Remote sensing (Basel, Switzerland)*, *10*(9), 1484. https://doi.org/10.3390/rs10091484

Wang, P., Limpens, J., Nauta, A., van Huissteden, C., van Rijssel, S. Q., Mommer, L., de Kroon, H., Maximov, T. C., & Heijmans, M. M. P. D. (2018). Depth‐based differentiation in nitrogen uptake between graminoids and shrubs in an Arctic tundra plant community. *Journal of vegetation science*, *29*(1), 34-41. https://doi.org/10.1111/jvs.12593

Wich, S. A., & Koh, L. P. (2018). *Conservation Drones: Mapping and Monitoring Biodiversity*. Oxford: Oxford University Press. https://doi.org/10.1093/oso/9780198787617.001.0001

Yao, X., Wang, N., Liu, Y., Cheng, T., Tian, Y., Chen, Q., & Zhu, Y. (2017). Estimation of Wheat LAI at Middle to High Levels Using Unmanned Aerial Vehicle Narrowband Multispectral Imagery. *Remote sensing (Basel, Switzerland)*, *9*(12), 1304. https://doi.org/10.3390/rs9121304

Zeileis, A., Cribari-Neto, F., Gruen, B., Kosmidis, I., Simas, A. B., & Rocha, A. V. (2021). *Beta Regression*. Retrieved 24.02.2022 from https://cran.r-project.org/web/packages/betareg/betareg.pdf

Zuur, A. F. (2009). *Mixed effects models and extensions in ecology with R*. Springer.

7 Appendices

Appendix 1 – Overall effect table

Table 1A Median, mean, maximum and minimum values (in percentage) for all vegetation groups for both cadaver sites and control sites. Cad = cadaver sites, Con= control sites. P-value from the Wilcoxon signed ranked test for each vegetation groups at cadaver sites compared to control sites.

Vegetation groups	**Median Cad**	**Mean Cad**	**Min Cad**	**Max Cad**	**Median Con**	**Mean Con**	**Min Con**	**Max Con**	**P-value**
Woody plants	10.00	11.90	0.00	25.00	15.00	12.79	0.00	20.00	0.472
Graminoids	15.00	17.07	5.00	35.00	15.00	13.66	1.00	25.00	0.007
Herbs	15.00	15.17	5.00	25.00	15.00	15.34	5.00	20.00	0.644
Bryophytes	20.00	21.72	5.00	40.00	25.00	26.72	5.00	50.00	0.004
Lichen	10.00	7.76	0.00	20.00	10.00	10.17	0.00	50.00	0.066

Appendix 2 - Model selections glmm models

Woody plants

Table 2A Results from the model selection for woody plants with only the new cadaver and control sites (only 2021).

Model	Df	AICc	ΔAICc	AICcWt
Woody plant cover ~ Type	4	-1006.0	0.00	0.745
Woody plant cover ~ Type + Band	6	-1002.7	3.31	0.142
Woody plant cover ~ Type * Band	8	-1001.5	4.55	0.077
Woody plant cover ~ 1	3	-999.6	6.42	0.030
Woody plant cover ~ Band	5	-996.4	9.61	0.006

Table 2B Results from the model selection for woody plants with the old cadaver and control sites (2020, 2019 and 2017).

Model	Df	AICc	ΔAICc	AICcWt
Woody plant cover ~ Type * Band	8	-3849.1	0.00	0.673
Woody plant cover ~ Type + Band	6	-3847.3	1.85	0.267
Woody plant cover ~ Band	5	-3843.1	6.04	0.033
Woody plant cover ~ Type	4	-3842.5	6.59	0.025
Woody plant cover ~ 1	3	-3837.9	11.23	0.002

Graminoids

Table 2C Results from the model selection for graminoids with only the new cadaver and control sites (only 2021).

Model	Df	AICc	ΔAICc	AICcWt
Graminoid cover ~ Type	4	-1299.6	0.00	0.843
Graminoid cover ~ Type + Band	6	-1295.9	3.61	0.139
Graminoid cover ~ Type * Band	8	-1291.8	7.74	0.018
Graminoid cover ~ 1	3	-1256.4	43.12	0.000
Graminoid cover ~ Band	5	-1252.8	46.73	0.000

Table 2D Results from the model selection for graminoids with the old cadaver and control sites (2020, 2019 and 2017).

Model	Df	AICc	ΔAICc	AICcWt
Graminoid cover ~ Type * Band	8	-15302.1	0.00	1
Graminoid cover ~ Type + Band	6	-15283.7	18.43	0
Graminoid cover ~ Band	5	-15241.5	60.60	0
Graminoid cover ~ Type	4	-15241.2	60.87	0
Graminoid cover ~ 1	3	-15204.4	97.72	0

Herbs

Table 2E Results from the model selection for herbs with only the new cadaver and control sites (only 2021).

Model	Df	AICc	ΔAICc	AICcWt
Herb cover ~ Type * Band	8	-1105.0	0.00	0.890
Herb cover ~ Type	4	-1099.8	5.18	0.067
Herb cover ~ Type + Band	6	-1098.9	6.05	0.043
Herb cover ~ 1	3	-1057.9	47.06	0.000
Herb cover ~ Band	5	-1057.8	47.23	0.000

Table 2F Results from the model selection for herbs with the old cadaver and control sites (2020, 2019 and 2017).

Model	Df	AICc	ΔAICc	AICcWt
Herb cover ~ 1	3	-3453.1	0.00	0.550
Herb cover ~ Type	4	-3451.5	1.53	0.255
Herb cover ~ Band	5	-3450.1	2.95	0.126
Herb cover ~ Type + Band	6	-3448.6	4.47	0.059
Herb cover ~ Type * Band	8	-3445.2	7.91	0.011

Bryophytes

Table 2G Results from the model selection for bryophytes with only the new cadaver and control sites (only 2021).

Model	Df	AICc	ΔAICc	AICcWt
Bryophyte cover ~ Type * Band	8	-811.1	0.00	0.977
Bryophyte cover ~ Type + Band	6	-803.0	8.08	0.017
Bryophyte cover ~ Type	4	-800.0	11.06	0.004
Bryophyte cover ~ Band	5	-798.3	12.77	0.002
Bryophyte cover ~ 1	3	-794.9	16.20	0.000

Table 2H Results from the model selection for bryophytes with the old cadaver and control sites (2020, 2019 and 2017).

Model	Df	AICc	ΔAICc	AICcWt
Bryophyte cover ~ Type * Band	8	-14387.8	0.00	1
Bryophyte cover ~ Type + Band	6	-14355.5	32.24	0
Bryophyte cover ~ Type	4	-14288.9	98.84	0
Bryophyte cover ~ Band	5	-14283.6	104.19	0
Bryophyte cover ~ 1	3	-14214.1	173.67	0

Lichen

Table 2I Results from the model selection for lichen with only the new cadaver and control sites (only 2021).

Model	Df	AICc	ΔAICc	AICcWt
Lichen cover ~ Type * Band	8	-1202.0	0.00	0.695
Lichen cover ~ Type + Band	6	-1200.1	1.94	0.263
Lichen cover ~ Type	4	-1196.3	5.72	0.040
Lichen cover ~ Band	5	-1190.5	11.50	0.002
Lichen cover ~ 1	3	-1185.5	16.53	0.000

Table 2J Results from the model selection for lichen with the old cadaver and control sites (2020, 2019 and 2017).

Model	Df	AICc	ΔAICc	AICcWt
Lichen cover ~ Type * Band	8	-16300.9	0.00	1
Lichen cover ~ Type + Band	6	-16275.1	25.82	0
Lichen cover ~ Type	4	-16267.7	33.21	0
Lichen cover ~ Band	5	-16207.9	92.97	0
Lichen cover ~ 1	3	-16198.0	102.90	0

Appendix 3 - RGBVI

Table 3A Results from the Wilcoxon Signed Rank Test performed for the RGBVII for both old and new sites at 30 m, 50 m, and 100 m altitude.

RGBVI (Red Green Blue Vegetation Index)		
Grid	P-value new sites	P-value old sites
Core 30 m	0.107	< 0.001
Inner 30 m	0.058	< 0.001
Outer 30 m	0.141	0.008
Total 30 m	0.107	<. 0.001
Core 50 m	0.021	< 0.001
Inner 50 m	0.014	< 0.001
Outer 50 m	0.042	0.132
Total 50 m	0.021	0.001
Core 100 m	0.021	< 0.001
Inner 100 m	0.021	< 0.001
Outer 100 m	0.042	0.146
Total 100 m	0.030	0.003

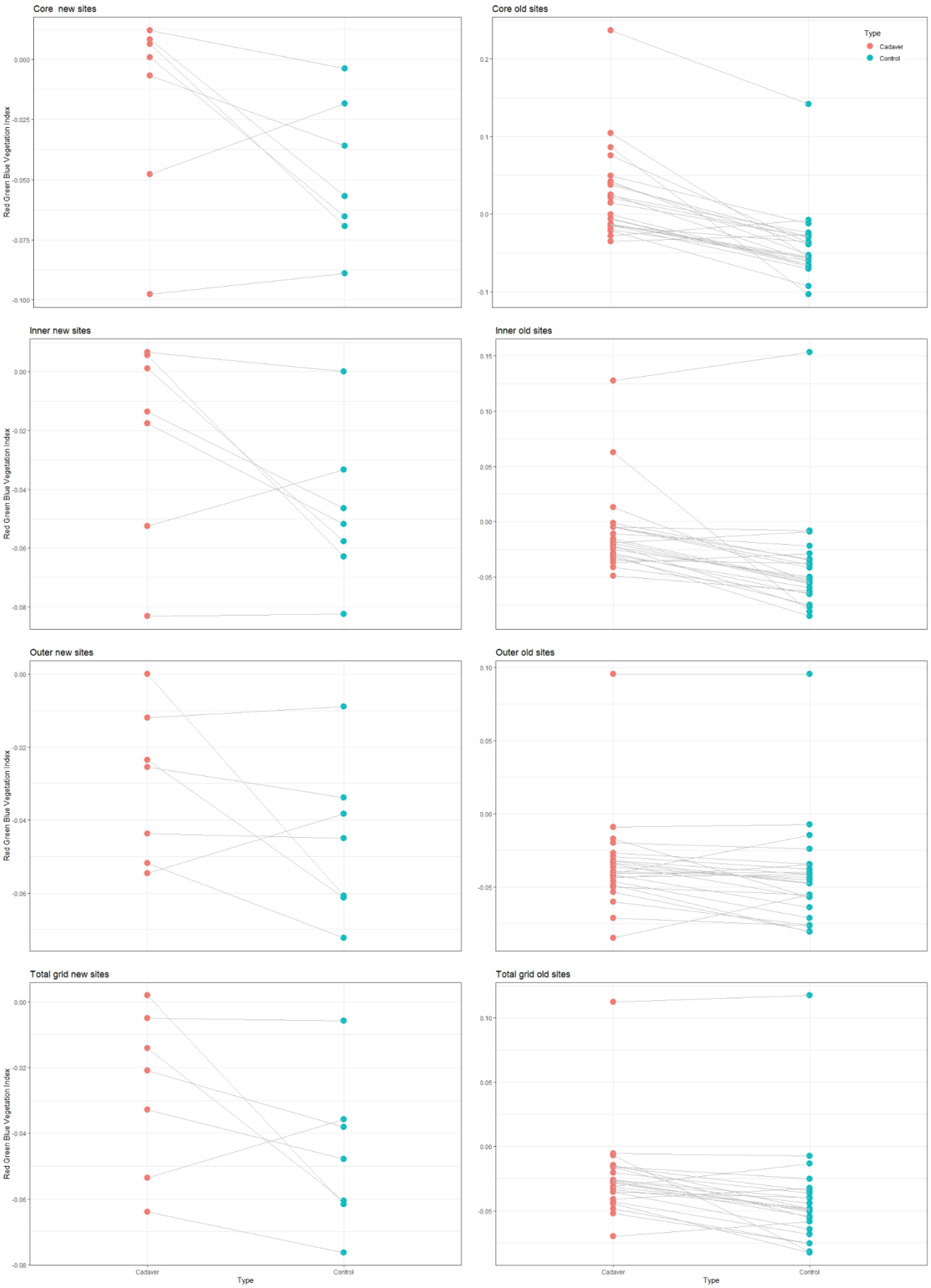

Figure 3B RGBVI index values at 30 m altitude. (left column), (right column). The gray lines connect cadaver sites with the paired control sites.

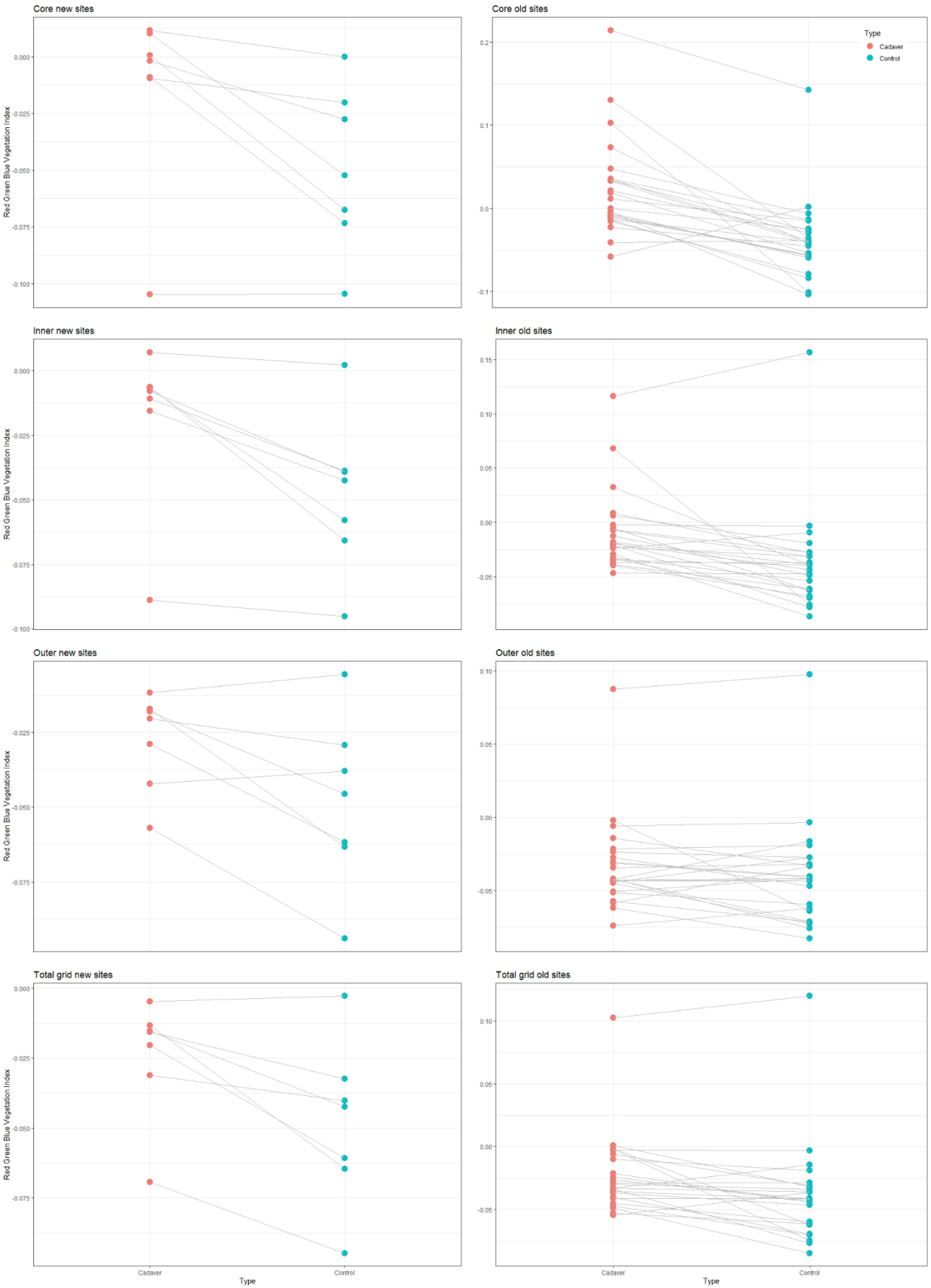

Figure 3C RGBVI index values at 50 m altitude. (left column), (right column). The gray lines connect cadaver sites with the paired control sites

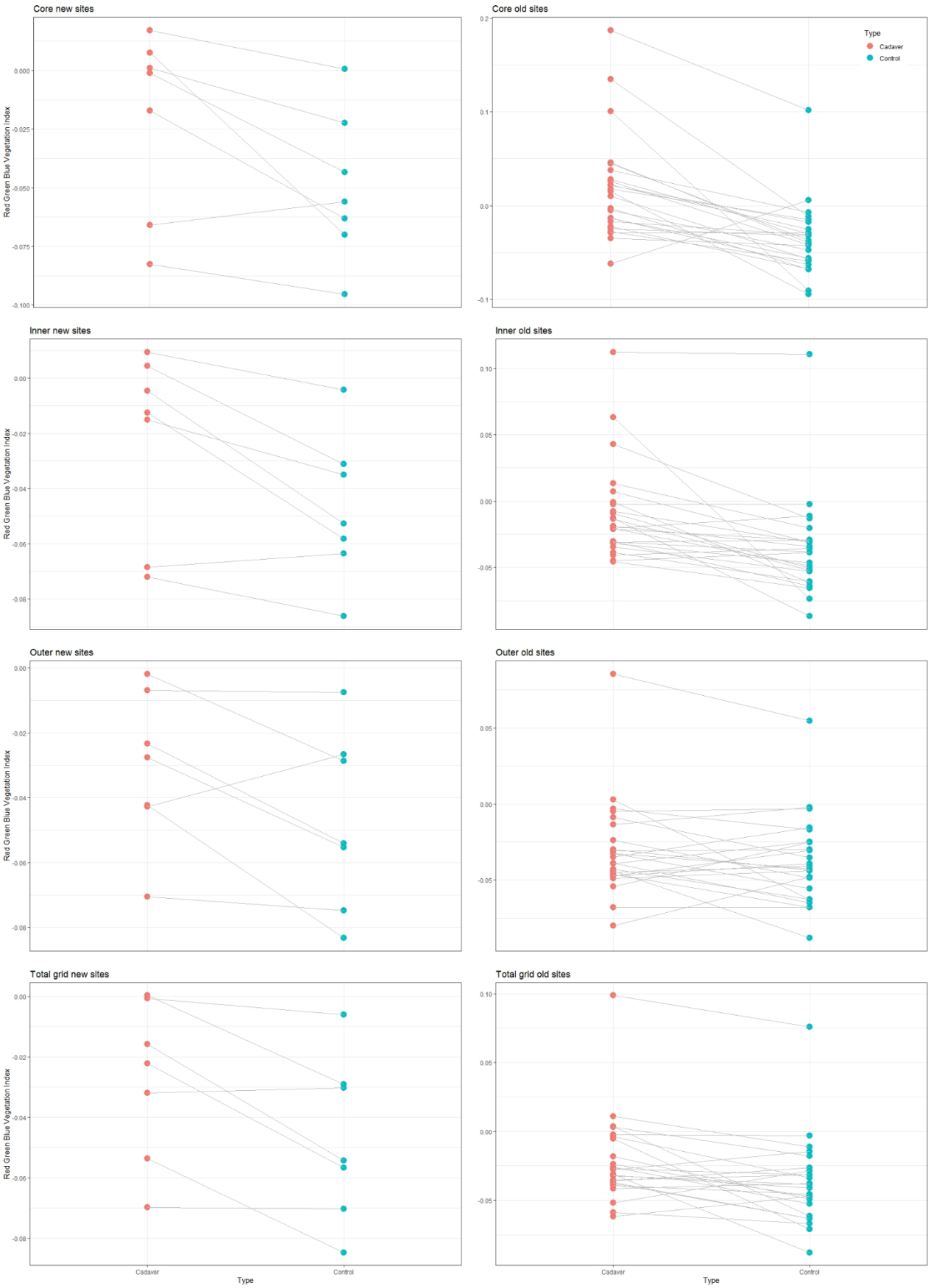

Figure 3D RGBVI index values at 100 m altitude. (left column), (right column). The gray lines connect cadaver sites with the paired control site

Appendix 4 – MGRVI

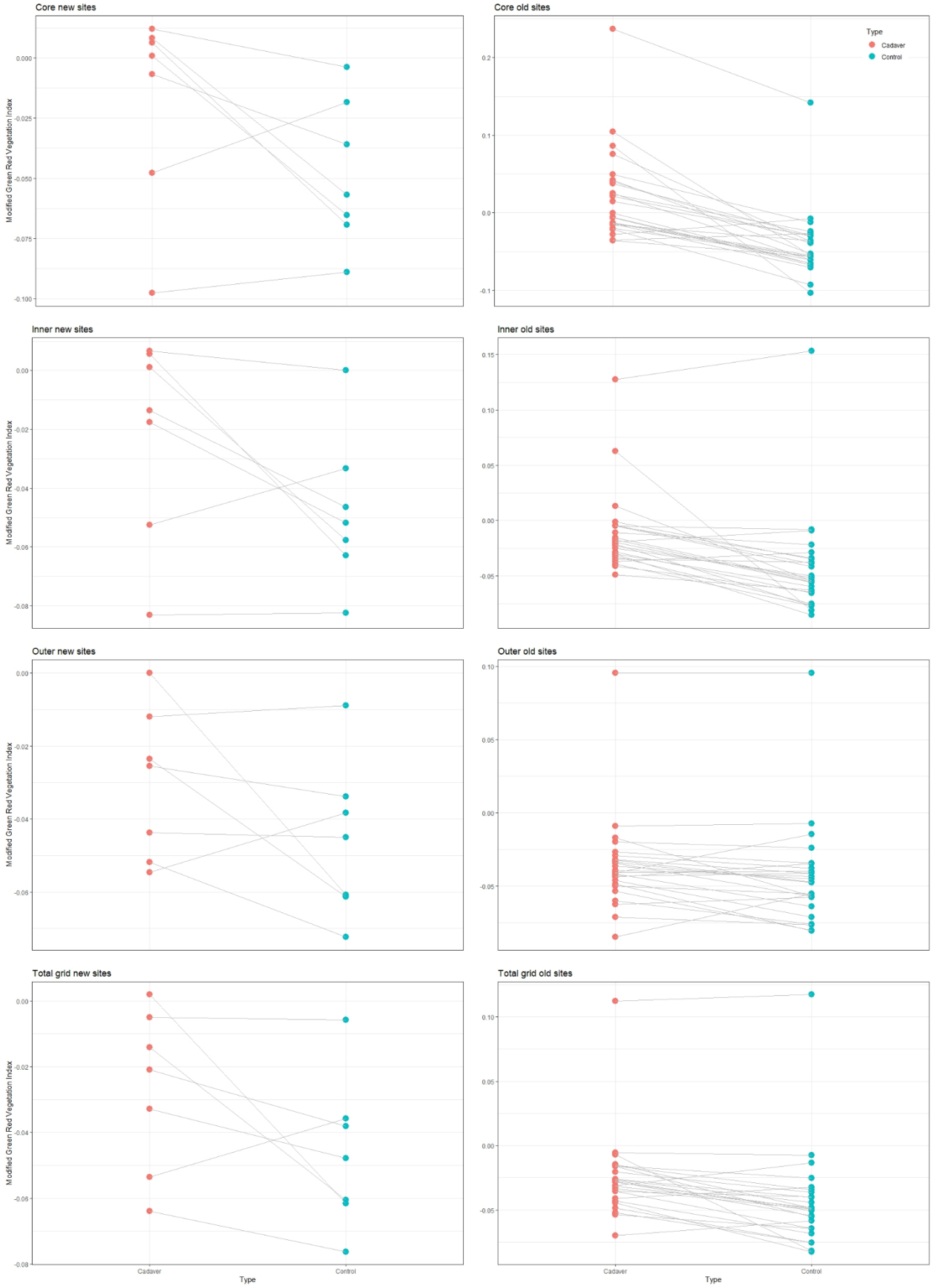

Figure 4A MGRVI index values at 30 m altitude. (left column), (right column). The gray lines connect cadaver sites with the paired control sites.

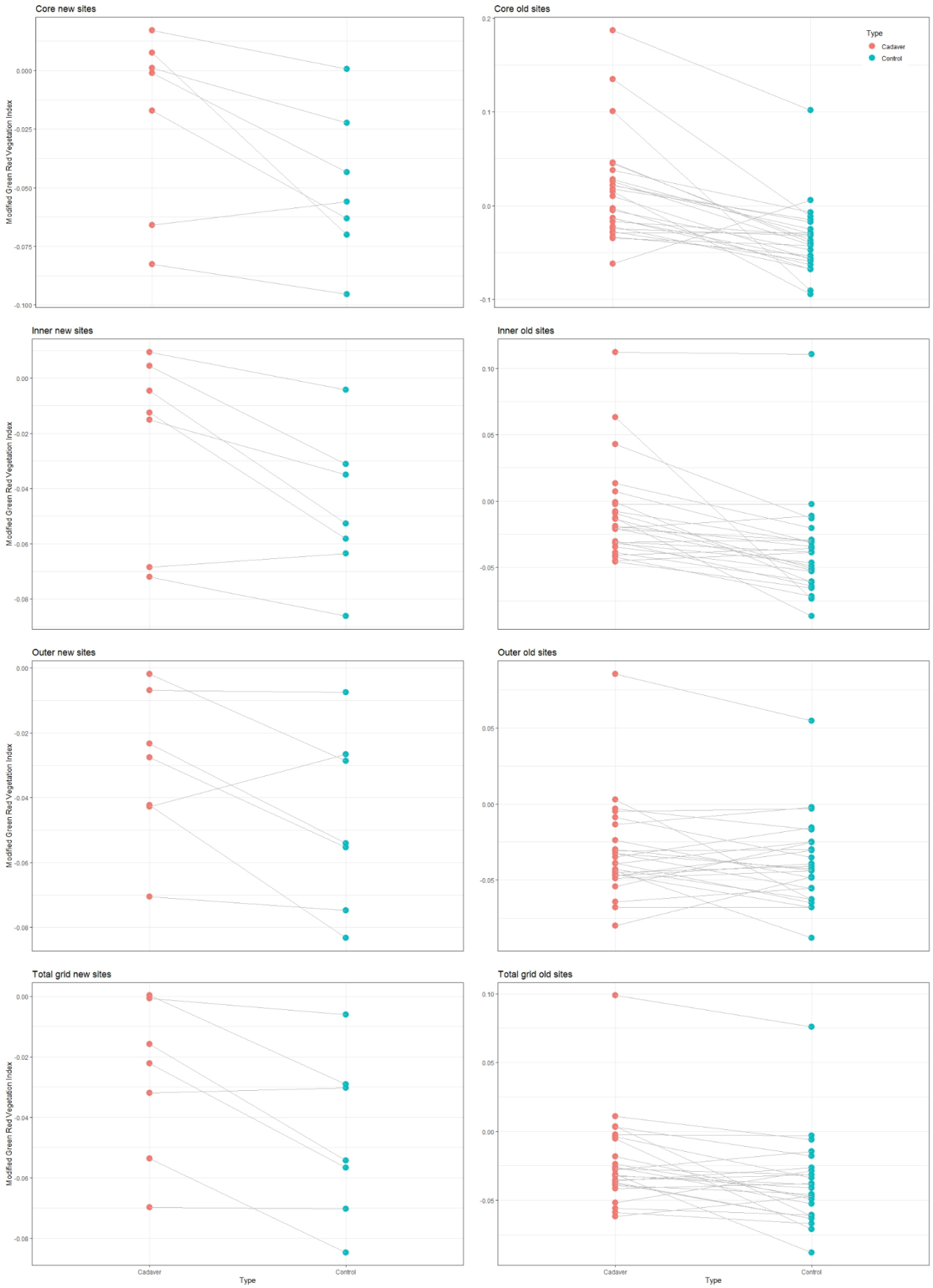

Figure 3B MGRVI index values at 100 m altitude. (left column), (right column). The gray lines connect cadaver sites with the paired control sites.

Appendix 5 – GLI

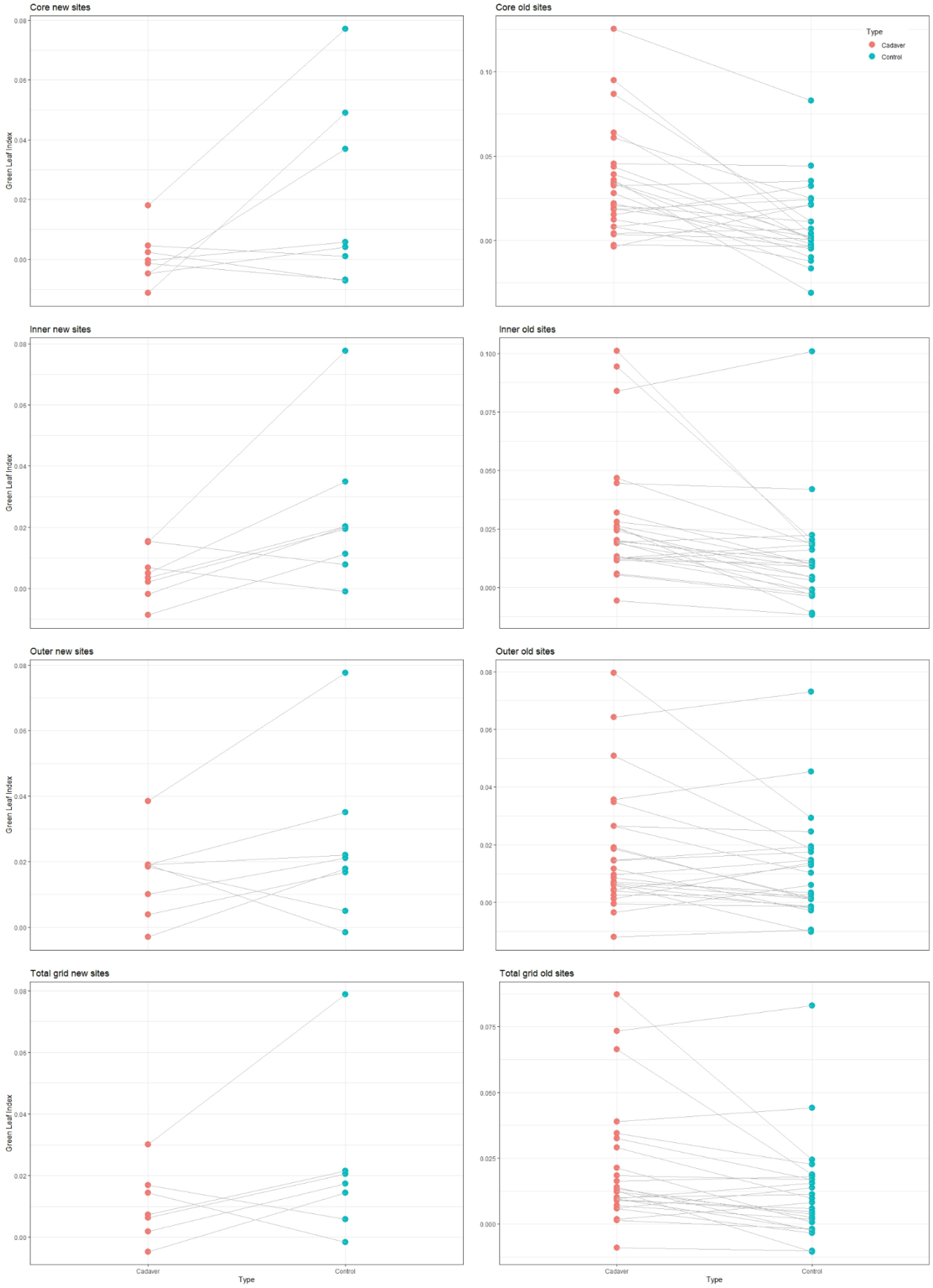

Figure 5A GLI index values at 30 m altitude. (left column), (right column). The gray lines connect cadaver sites with the paired control sites

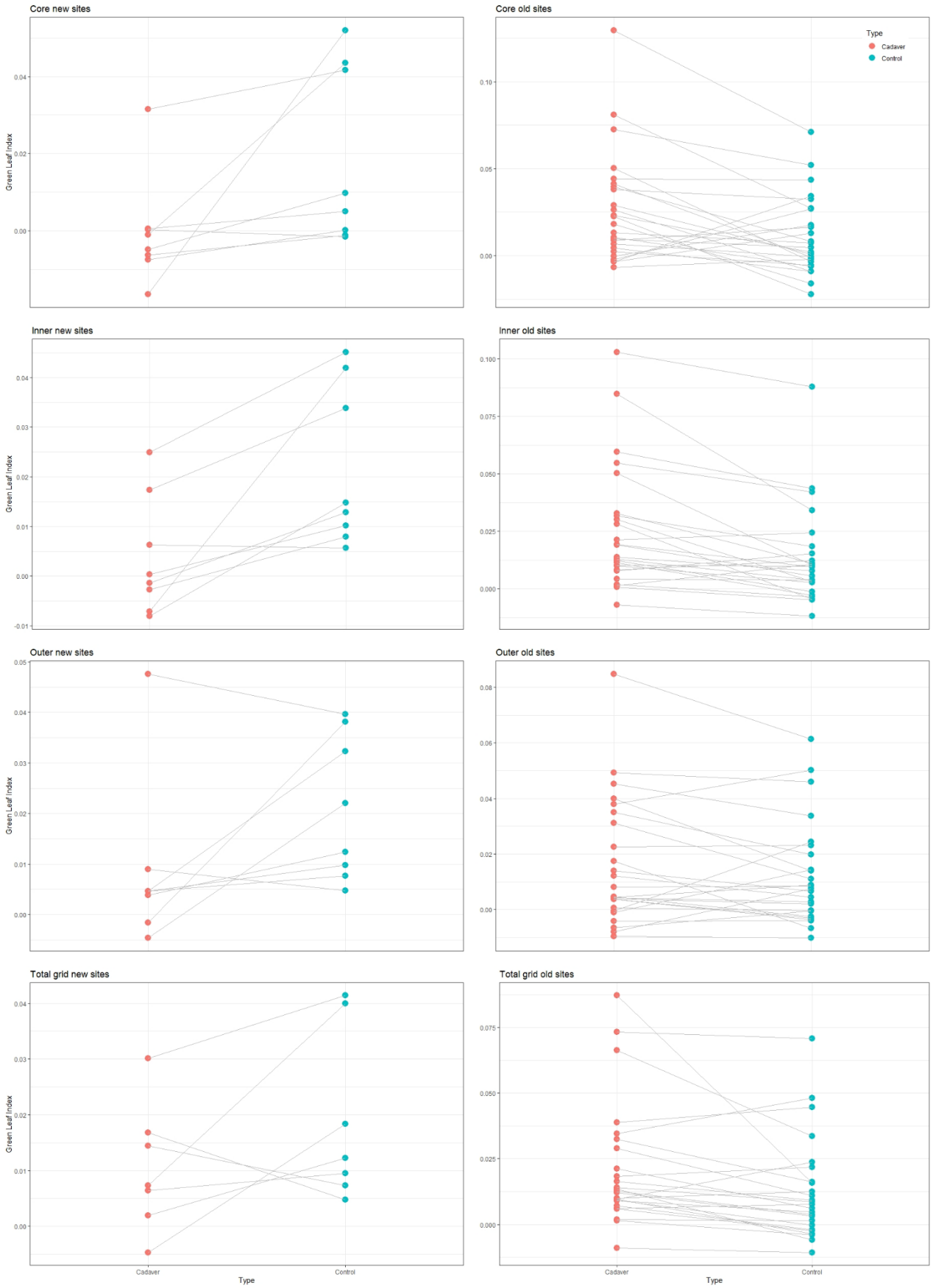

Figure 5B GLI index values at 100 m altitude. (left column), (right column). The gray lines connect cadaver sites with the paired control sites